



UNIVERSIDADE DE SÃO PAULO
FACULDADE DE CIÊNCIAS FARMACÊUTICAS DE RIBEIRÃO PRETO

Structural and biochemical characterization of *Schistosoma mansoni* class II fumarate hydratase enzyme

Caracterização estrutural e bioquímica da enzima fumarato hidratase classe II de *Schistosoma mansoni*

IARA AIMÊ CARDOSO

Ribeirão Preto
2019

UNIVERSIDADE DE SÃO PAULO
FACULDADE DE CIÊNCIAS FARMACÊUTICAS DE RIBEIRÃO PRETO

IARA AIMÊ CARDOSO

Structural and biochemical characterization of *Schistosoma mansoni* class II fumarate hydratase enzyme

Caracterização estrutural e bioquímica da enzima fumarato hidratase classe II de *Schistosoma mansoni*

Master dissertation presented to the Graduate Program of School of Pharmaceutical Sciences of Ribeirão Preto/USP for the degree of Master in Sciences.

Concentration Area: Chemistry and Biological Physics

Supervisor: Profa. Dra. Maria Cristina Nonato

Corrected version of master dissertation presented to the Pharmaceutical Sciences Graduate Program, on 08/11/2019. The original version is available at School of Pharmaceutical Sciences of Ribeirão Preto/USP.

Ribeirão Preto
2019

I AUTHORIZE THE REPRODUCTION AND TOTAL OR PARTIAL DISCLOSURE OF THIS WORK, BY ANY CONVENTIONAL OR ELECTRONIC MEANS

Cardoso, Iara Aimê

Structural and biochemical characterization of *Schistosoma mansoni* class II fumarate hydratase enzyme. Ribeirão Preto, 2019.

64 p.; 30 cm.

Master dissertation presented to the Graduate Program of School of Pharmaceutical Sciences of Ribeirão Preto/USP for the degree of Master in Sciences. Concentration Area: Chemical and Biological Physics

Supervisor: Nonato, Maria Cristina

1. Fumarate hydratase 2. *Schistosoma mansoni* 3. X-ray crystallography 4. Kinetic assay

APPROVAL PAGE

Iara Aimê Cardoso

Structural and biochemical characterization of *Schistosoma mansoni* class II fumarate hydratase enzyme

Master dissertation presented to the Graduate Program of School of Pharmaceutical Sciences of Ribeirão Preto/USP for the degree of Master in Sciences.

Concentration Area: Chemistry and Biological Physics

Supervisor: Prof. Dr. Maria Cristina Nonato

Approved on:

Examiners

Prof. Dr. _____

Institution: _____ Signature: _____

Agradecimentos

Gostaria de agradecer ao meu namorado Pedro, que está sempre ao meu lado me incentivando e me apoiando, mesmo nos momentos mais difíceis. Obrigada por sempre acreditar em mim.

Aos meus pais e irmãs (Mário, Rosa, Isis e Ieda) que me incentivaram a sempre buscar o melhor de mim.

À família Campiteli (Cleiza, Edison e Henrique) por todos os momentos em que me apoiaram durante o mestrado.

Agradeço à minha orientadora Profa. Maria Cristina Nonato pelas discussões enriquecedoras e pela oportunidade de desenvolver esse lindo trabalho.

Agradeço imensamente aos meus amigos do LCP-RP, por todo o suporte, ajuda e parceria durante essa jornada. Em especial às minhas amigas Mariana e Marília que muito contribuíram com todo o apoio, discussões e bons momentos.

Aos ex-alunos do LCP-RP (Ricardo, Joane, Renata, Matheus e Paty) e a ex-funcionária Juliana, pelos ensinamentos e discussões científicas, e em especial à Aline, que teve participação no início deste trabalho.

Ao pessoal do Laboratório de Toxinas Animais (Karla, Gisele, Isadora, Ernesto, Isabela, Fran e Beatriz), por todo o suporte e compreensão.

À professora Eliane Candiani Arantes Braga pelo incentivo e por todos os ensinamentos.

Agradeço à Professora Renata Viana Lopes por gentilmente disponibilizar o equipamento Zetasizer.

Agradeço também à FCFRP pela oportunidade de desenvolver meu projeto de mestrado nesta maravilhosa instituição pública e de extrema qualidade.

O presente trabalho foi realizado com apoio da Coordenação de Aperfeiçoamento de Pessoal de Nível Superior – Brasil (CAPES) – Código de Financiamento 001.

"Se você procura se encontrar, não olhe para um espelho, pois lá não há nada além de uma
sombra, um estranho..."

Silenius

Abstract

Cardoso, I. A. **Structural and biochemical characterization of *Schistosoma mansoni* class II fumarate hydratase enzyme.** 2019. 64f. Dissertation (Master). Faculdade de Ciências Farmacêuticas de Ribeirão Preto – Universidade de São Paulo, Ribeirão Preto, 2019.

Schistosomiasis is a neglected tropical disease caused by trematode worms from the genus *Schistosoma*. Schistosomiasis is the second most devastating parasitic disease after malaria. The disease has a high economic burden and affects mainly poor population without access to proper sanitation. Praziquantel is the only drug approved for the treatment of schistosomiasis and resistance is already reported. Fumarate hydratases or fumarases are enzymes that catalyze the reversible hydration of fumarate to L-malate. This enzyme participates in DNA repair and important metabolic processes such as the urea and the tricarboxylic acid cycles. Fumarases are divided in two classes, and *Schistosoma mansoni* possess both, being class I localized in mitochondria, while class II is cytosolic. The fundamental role of fumarases in the metabolism make them potential target for drug design against schistosomiasis. This work describes, for the first time, the cloning, expression and purification protocol for the class II fumarate hydratase from *Schistosoma mansoni* (*SmFH_{II}*). In order to estimate the contribution of the reverse reaction, the enzyme was kinetically characterized using both substrates concomitantly. *SmFH_{II}* was shown to follow a Michaelis-Menten mechanism of catalysis with k_{cat}^{MAL} of $19 \text{ mM}^{-1}\text{s}^{-1}$ and k_{cat}^{FUM} of $49 \text{ mM}^{-1}\text{s}^{-1}$, and K_m^{MAL} of 0.56 mM and K_m^{FUM} of 0.15 mM . Differential scanning fluorimetry (DSF) performed under different chemical environments shows that the highest thermal stability is reached at pH 7.5 and at higher ionic strength. The significant thermoshift observed for *SmFH_{II}* in presence of well known ligands makes DSF the adequate technique for ligand screening. *SmFH_{II}* structure in complex with L-malate was determined by single crystal X-ray diffraction, at 1.85 \AA resolution. A new construct [*SmFH_{II}*($\Delta_{263-277}$)] lacking the additional portion only found in trematode worms was also evaluated by kinetic and DSF experiments. Although not essential for activity, the results suggest that the removal of this region impacts on protein stability and may have influence on L-malate catalysis. The differences between *SmFH_{II}* and human fumarase are distributed all over the structure, and could be explored to design new selective inhibitors.

Keywords: Fumarate hydratase, *Schistosoma mansoni*, X-ray crystallography, kinetic characterization.

Resumo

Cardoso, I. A. **Caracterização estrutural e bioquímica da enzima fumarato hidratase classe II de *Schistosoma mansoni***. 2019. 64f. Dissertação (Mestrado). Faculdade de Ciências Farmacêuticas de Ribeirão Preto – Universidade de São Paulo, Ribeirão Preto, 2019.

A esquistossomose é uma doença tropical negligenciada causada por parasitas trematódeos do gênero *Schistosoma*. A esquistossomose é a segunda doença parasitária mais devastadora do mundo, atrás apenas da malária. A doença tem um alto impacto econômico, afetando principalmente a população pobre sem acesso a saneamento adequado. Praziquantel é o único medicamento aprovado para o tratamento da esquistossomose e já existem relatos de parasitas resistentes a esse fármaco. Fumarato hidratases ou fumarases são enzimas que catalisam a hidratação reversível de fumarato em L-malato. Essa enzima participa do reparo ao dano do DNA e de processos metabólicos importantes, como os ciclos da uréia e do ácido tricarbóxico. As fumarases são divididas em duas classes e o *S. mansoni* possui ambas, sendo a classe I mitocondrial, enquanto a classe II é citosólica. O papel fundamental da fumarase no metabolismo faz dela um alvo potencial para o planejamento de fármacos contra a esquistossomose. Este trabalho descreve, pela primeira vez, o protocolo de clonagem, expressão e purificação da fumarato hidratase classe II de *Schistosoma mansoni* ($SmFH_{II}$). De forma a estimar a contribuição da reação reversa, a enzima foi caracterizada cineticamente utilizando os dois substratos concomitantemente. A $SmFH_{II}$ demonstrou seguir o mecanismo de catálise de Michaelis-Menten, tendo um k_{cat}^{MAL} de $19 \text{ mM}^{-1} \text{ s}^{-1}$ e k_{cat}^{FUM} de $49 \text{ mM}^{-1} \text{ s}^{-1}$, e K_m^{MAL} de $0,56 \text{ mM}$ e K_m^{FUM} de $0,15 \text{ mM}$. Fluorimetria de varredura diferencial (DSF) realizada em diferentes ambientes químicos demonstrou que a maior estabilidade térmica da proteína é alcançada em pH 7,5 e também com o aumento alta força iônica, além de ser uma técnica útil para a triagem de ligantes. A estrutura da $SmFH_{II}$ foi determinada por difração de raios-X de monocristal, com uma resolução de $1,85 \text{ \AA}$. Uma nova construção [$SmFH_{II(\Delta 263-277)}$] sem a porção adicional, encontrada apenas em vermes de trematódeos, também foi avaliada por ensaios cinéticos e de DSF. Embora não seja essencial para a atividade enzimática, os resultados sugerem que a remoção dessa região afeta a estabilidade da proteína e pode ter influência na catálise do L-malato. As diferenças entre $SmFH_{II}$ e fumarase humana estão distribuídas por toda a estrutura e podem ser exploradas para delinear novos inibidores seletivos.

Palavras-chave: Fumarato hidratase, *Schistosoma mansoni*, cristalografia de raios-x, caracterização cinética.

List of Figures

Figure 1. Distribution of schistosomiasis, according to the positivity range - Brazil, 2010 - 2015.	3
Figure 2. Schistosoma spp. life cycle scheme.	4
Figure 3. Schistosome worm pair.	5
Figure 4. Reversible reaction catalyzed by fumarase enzyme.	7
Figure 5. Sequence alignment of class II fumarases. SmFHII (<i>S. mansoni</i>), SjFH (<i>S. japonicum</i>), FhFHII (<i>Fasciola hepatica</i>), CsFHII (<i>Clonorchis sinensis</i>), HsFH (<i>Homo sapiens</i>), FumC (<i>Escherichia coli</i>), MtFH (<i>Mycobacterium tuberculosis</i>).	8
Figure 6. Fumarase structure encoded by Rv1098c <i>Mycobacterium tuberculosis</i> gene.	9
Figure 7. Optimized codon of open reading frame for the putative class II <i>Schistosoma mansoni</i> fumarase based on the sequence available in GenBank (Uniprot ID: G4LVG5).	13
Figure 8. Alignment between the predicted protein (Uniprot ID G4LVG5) and the correct amino acid sequence of class II fumarate hydratase from <i>S. mansoni</i> (SmFHII_correct).	18
Figure 9. 14% SDS-PAGE representing all steps of SmFH _{II} purification using an affinity column (Ni-NTA agarose resin).	19
Figure 10. 14% SDS-PAGE representing all steps of SmFH _{II(Δ263-277)} purification using an affinity column (Ni-NTA agarose resin).	20
Figure 11. Oligomeric state determination of recombinant SmFH _{II} and SmFH _{II(Δ263-277)} by gel filtration.	20
Figure 12. Mass distribution of light scattered by protein solution as a function of particle diameter.	21
Figure 13. Thermostability assay for SmFH _{II} and SmFH _{II(Δ263-277)} comparing pH versus salt concentration.	22
Figure 14. Enzyme activity measured as a function of pH.	23
Figure 15. Surface graph of complete steady-state kinetics of SmFH _{II} (A), SmFH _{II(Δ263-277)} (B) and HsFH (C) with both substrates (L-malate and fumarate) simultaneously.	24
Figure 16. SmFH _{II} crystals.	25
Figure 17. Crystal structure of SmFH _{II} solved by molecular replacement (data resolution: 1.85 Å).	28
Figure 18. Protuberant additional portion of SmFH _{II}	29
Figure 19. The catalytic pocket.	30

Figure 20. RMSD versus residue.....	31
Figure 21. Ligands bound to SmFH _{II} structure.....	34
Figure 22. Main differences between SmFH _{II} and HsFH (5UPP) electrostatic potential surface.....	36
Figure 23. C-terminal closed and open state.	37

List of Tables

Table 1. Oligonucleotide primers used in overlap extension polymerase chain reaction.....	12
Table 2. Kinetics parameters* obtained in the steady-state kinetic with both substrates (L-malate and fumarate).	24
Table 3. Data collection and refinement statistics.	26

List of Abbreviations

DLS	Dynamic light scattering
DALYs	Disability-adjusted life years
DDR	DNA damage response
DMSO	Dimethyl Sulfoxide
DSB	DNA double strand break
DSF	Differential scanning fluorimetry
FH_I	Class I fumarate hydratase or fumarase
FH_{II}	Class II fumarate hydratase or fumarase
FIOCRUZ	<i>Fundação Oswaldo Cruz</i>
FUM	Fumarate
FumC	<i>Escherichia coli</i> class II fumarase
HsFH	Human fumarase
IPTG	isopropyl β -D-1-thiogalactopyranoside
kDa	kiloDalton
LB	Luria Bertani
LmFH	<i>Leishmania major</i> fumarase
MAL	L-malate
MtFH	<i>Mycobacterium tuberculosis</i> fumarase
NTD	Neglected tropical disease
PCR	Polymerase Chain Reaction
PDB	Protein Data Bank

PEG	Polyethylene glycol
PMSF	Phenylmethylsulfonyl fluoride
Sm	<i>Schistosoma mansoni</i>
SmFH_I	<i>Schistosoma mansoni</i> class I fumarase
SmFH_{II}	<i>Schistosoma mansoni</i> class II fumarase
SUMO	Small Ubiquitin Modifier
SUS	<i>Sistema Único de Saúde</i>
TCA	Tricarboxylic acid cycle
TcFH	<i>Trypanosoma cruzi</i> fumarase
ULP1	Ubiquitin like protease 1
WHO	World Health Organization

Summary

Abstract	i
Resumo	ii
List of Figures	iii
List of Tables.....	v
1. INTRODUCTION.....	1
1.1. Neglected tropical diseases	1
1.2. Schistosomiasis	1
1.2.1. History.....	1
1.2.2. Epidemiology	2
1.2.3. Infection and transmission	3
1.2.4. Symptoms, diagnosis, and treatment.....	5
1.3. Fumarate Hydratase	7
1.3.1. Fumarase as a target to schistosomiasis	10
2. OBJECTIVES	11
3. MATERIALS AND METHODS	11
3.1. Gene cloning of <i>SmFH_{II}</i>	11
3.2. Protein expression and purification	14
3.3. Size exclusion chromatography and DLS experiments	15
3.4. Differential Scanning Fluorimetry.....	15
3.5. Kinetics assay	16
3.6. X-ray crystallography	17
4. RESULTS.....	17
4.1. <i>SmFH_{II}</i> production and oligomeric characterization	17
4.2. DSF analysis	21
4.3. Optimum pH and kinetics assay	23
4.4. Overall structure of <i>SmFH_{II}</i>	25
5. DISCUSSION	31
6. CONCLUSION.....	39
7. REFERENCES.....	40
APPENDICES.....	48

1. INTRODUCTION

1.1. Neglected tropical diseases

The term neglected tropical diseases (NTDs) emerged in the 20th century to describe a group of infectious diseases that were found endemic in the tropical and subtropical areas of the globe. NTDs specially affect the poorest population with no adequate sanitation and constant contact with infectious vectors^{1; 2}. These diseases cause important morbidity and mortality, being a serious public health problem in many countries of Africa, Asia, and Latin America³. NTDs also reflect the scarce investments in research and development of new therapies or programs to their control².

Currently, the World Health Organization (WHO) recognizes 20 diseases as NTDs, including schistosomiasis, Chagas disease, dengue and chikungunya, leishmaniasis, among others. These diseases affect more than one billion people, which represents one sixth of the world population¹.

Neglected tropical diseases cause huge human suffering and numerous cases of death, remaining a serious impediment to socioeconomic development¹. The indifference to these diseases only aggravates the scenario of global inequality, which shows the need to searching new drugs that are more effective and accessible to the low-income populations, as well as to encourage prevention and control programs for NTDs.

1.2. Schistosomiasis

1.2.1. History

Schistosomiasis (also known as bilharziasis) is a parasitic neglected disease caused by blood flukes (trematode worms) of the genus *Schistosoma*, that can cause acute and chronic disease⁴. The disease is recognized as one of the oldest still existing infections. *Schistosoma haematobium* eggs were found in Egyptian mummies as old as 5,000 years⁵, while *Schistosoma mansoni* eggs were found in a latrine dated AD 1450-1550 in France⁶. The parasite was first described by the german parasitologist Theodor Maximilian Bilharz in 1851 during an autopsy performed at Cairo, and it was firstly named *Distomum haematobium*.^{7; 8}

In Brazil, the first identification of *S. mansoni* worms was made by the doctor and researcher Manuel Augusto Pirajá da Silva in 1908⁹. The introduction of schistosomiasis in Brazil occurred through the trade of slaves originating from the west coast of Africa, who entered the country mainly through the ports of Recife and Salvador to work in sugarcane crops. The disease initially spread throughout the northeastern of Brazil, forming an extensive transmission area along the states of Rio Grande do Norte and Bahia. In the 18th century, with the decline of sugar production in the Northeast and the beginning of the gold and diamond cycle, an intense migratory flow introduced the disease in Minas Gerais state, and after that to the others states of Southeast region¹⁰.

1.2.2. Epidemiology

Schistosomiasis is second only to malaria as most devastating parasitic neglected disease in the world³. The disease has been reported from 78 countries, which affects almost 240 million people worldwide, and more than 700 million people live in endemic areas¹¹. The disease is prevalent in tropical and subtropical areas, and especially affects poor communities with no access to adequate sanitation and drinkable water¹². Furthermore, according to the number of disability-adjusted life years (DALYs), an important measure of overall disease burden, schistosomiasis resulted in losses of 1.4 million years of full health among global population in 2017¹³.

In Brazil, schistosomiasis is distributed over 19 states (**Figure 1**) and affects about 1.5 million individuals, with the highest incidence in the Northeast and Southeast regions¹⁴. Schistosomiasis in Brazil represents a great economic burden, and its major impact is related to productivity loss. It was estimated in Brazil a total cost of US\$ 41.7 million in 2015, with 94.6% belonging to indirect costs as leave, disease aid and premature dead¹⁵.

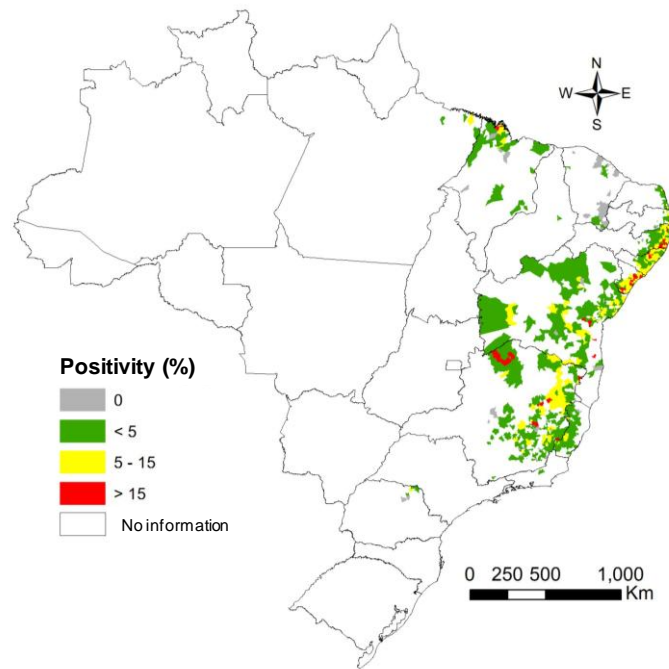


Figure 1. Distribution of schistosomiasis, according to the positivity range - Brazil, 2010 - 2015. (Extracted from Portal da saúde – SUS¹⁶).

1.2.3. Infection and transmission

Schistosomiasis is caused by the infection of dioecious trematode platelminths, and six species are capable of causing the disease in humans: *S. mekongi*, *S. intercalatum*, *S. guineensis*, *S. mansoni*, *S. haematobium* and *S. japonicum*. The last three species cited are responsible for the largest number of disease cases, and only *S. mansoni* is found in Brazil.

The transmission cycle (**Figure 2**) begins when *Schistosoma* eggs are eliminated with feces or urine, depending on the species. The eggs hatch, releasing the ciliated larval form, called miracidium, which swim and penetrate specific snail intermediate hosts (snail of the genus *Biomphalaria*, in Brazil). The stages in the snail include the generations of sporocysts and the asexual reproduction generating cercariae. The cercariae are released from the snail and penetrate the skin and/or mucous membranes, losing their forked tail and becoming schistosomulae. The schistosomulae migrate through venous circulation to the lungs and the heart till reach the liver and develop into sexed forms. Male and female adult worms exit the liver via the portal vein system when mature, copulate and reside in the mesenteric venules. *S. haematobium* most often inhabits in the vesicular and pelvic venous plexus of the bladder, but can also be found in the rectal venules. Finally, females release the

eggs in the small venules of the portal and perivesical systems. The eggs are moved through the lumen of the intestine (*S. mansoni*, *S. japonicum*, *S. mekongi*, *S. intercalatum/guineensis*) or the bladder and ureters (*S. haematobium*), and are eliminated with feces or urine, restarting the cycle³.

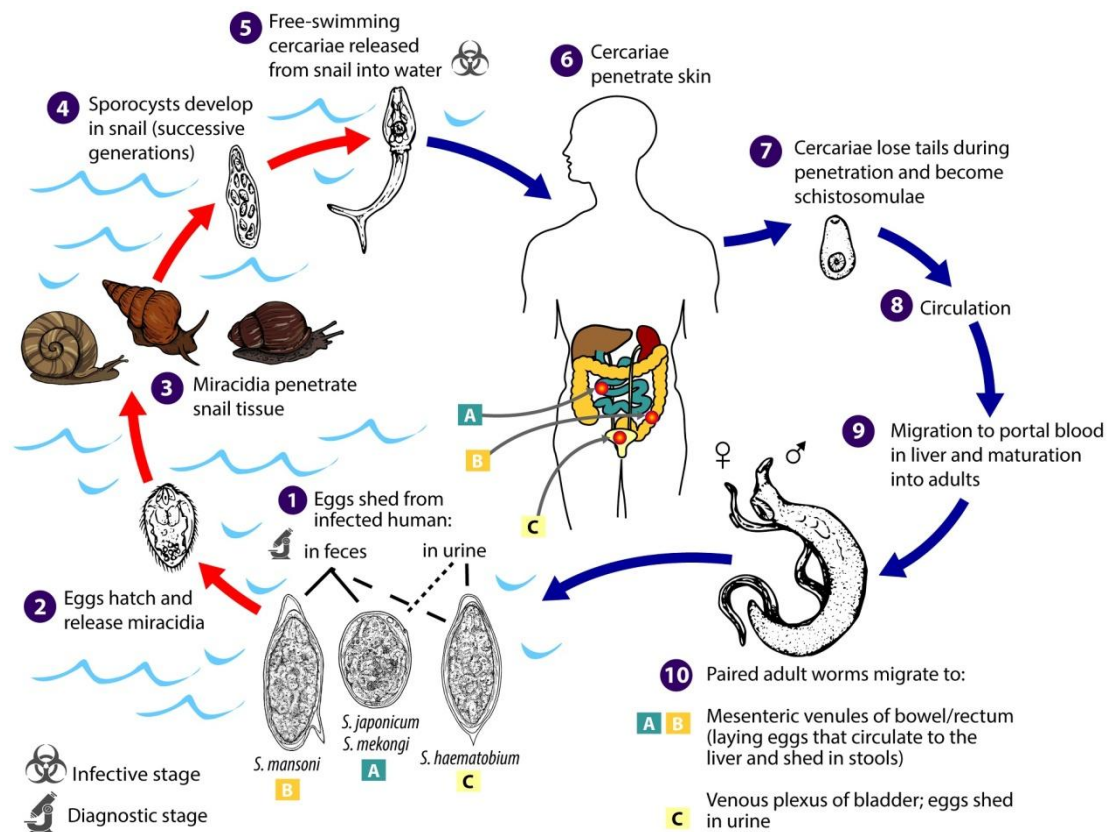


Figure 2. *Schistosoma* spp. life cycle scheme. (Extracted from Centers for Disease Control and Prevention³).

Male adult parasites are robust, tuberculate and measure approximately 6-12 mm in length and 10 mm in width (**Figure 3**). The female has a cylindrical body, slender and longer than male (7-17 mm in length)³ (**Figure 3**).

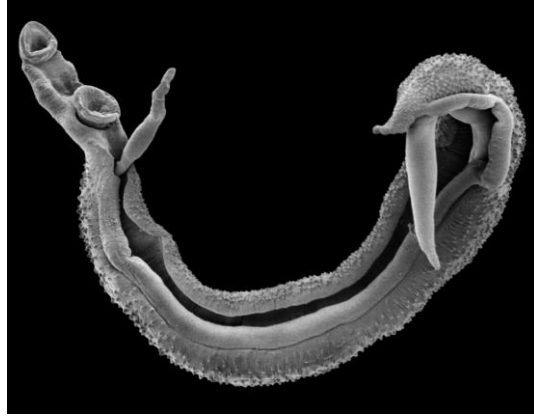


Figure 3. Schistosome worm pair. (Extracted from the Trustees of the Natural History Museum).

1.2.4. Symptoms, diagnosis, and treatment

Most people do not have any symptoms when they are first infected. Within a few days after infection, individuals may develop a rash or itchy skin, called cercariae dermatitis, characterized by reddish micropapules that resemble insect bites. About one to two months later, nonspecific symptoms appear, such as fever, headache, anorexia, nausea, asthenia, myalgia, cough and diarrhea, characterizing schistosomiasis in the acute form^{3; 14}.

The symptoms of schistosomiasis are not caused directly by the worms themselves, but due to the reaction of the immune system to the eggs. Eggs that are not eliminated by feces may lodge in the intestine, liver or bladder, causing inflammation and fibrosis³.

If not treated, schistosomiasis become chronic and can persist for years. In the chronic phase, the disease may have different manifestations, and the liver is the most frequently affected. Signs and symptoms of chronic schistosomiasis include: abdominal pain, enlarged liver, bloody stools, bloody urine, and problems passing urine. In the most severe form of the disease, eggs lodge in the brain or spinal cord and can cause seizures, paralysis, or inflammation of the spinal cord^{3; 14}.

The most commonly technique used for diagnosing schistosomiasis is the Kato-Katz method, which consists of identifying and counting the parasite's eggs in the feces or urine samples. Such method is a quick and simple way of diagnosis of the disease. Also, a serologic test (antibodies and/or antigens detected in blood samples) can be performed to confirm the infection^{3; 12; 14}.

Praziquantel is the only treatment for human schistosomiasis recommended by the World Health Organization. However, it fails to prevent immediate reinfection, a common feature of the disease for people who live in tropical areas with poor sanitary conditions.

Moreover, the emergence of drug resistant and praziquantel-insensitive parasites has increased due to its continuous and large-scale use for almost four decades^{17; 18; 19}. In Brazil, praziquantel is available as 600 mg tablets and it is administered orally as a single oral dose of 50 mg/kg for adults and 60 mg/kg for children¹⁰.

Although praziquantel have been used as large-scale treatment, also called preventive chemotherapy, its molecular mechanism of action remains unclear. Some studies suggest that schistosome worms calcium ion channels are the target of praziquantel, causing a rapid Ca^{2+} influx and severe spasms and paralysis of the worms' muscles^{20; 21; 22}. Other study demonstrated that praziquantel can cause morphological alterations (vacuolation and blebbing) near on the worm surface^{20; 23}.

Although there are no current commercially available vaccines for schistosomiasis, there are few initiatives for vaccine development in different stages of clinical trials^{24; 25; 26; 27}. One example is the Sm14/GLA-SE schistosomiasis vaccine, which has successfully completed phase I and phase IIa clinical trials, with phase IIb/III trials in progress. The vaccine was formulated with recombinant protein Sm14 and with glucopyranosyl lipid A (GLA) adjuvant in an oil-in-water emulsion (SE). Sm14 is a protein member of the fatty acid binding protein (FABP) family that plays an important role in the uptake, transport and compartmentalization of fatty acids from the host into the parasite, since helminths are not capable of synthesizing fatty acids by themselves. Besides being constituents of membranes, lipids also have important roles in the development of different lifecycle stages and the evasion of immune responses by adult worms and larvae. The research and development of Sm14/GLA-SE vaccine have been carried by the coordination of FIOCRUZ, a public institution linked to the Brazilian Ministry of Health²⁸.

Victims of schistosomiasis are concentrated in low and middle income country markets, and thus the disease remains away from the spotlights. With scarce investments in research dedicated to schistosomiasis, the world is far to achieve concrete improvements in prevention, treatment and quality of life for this representative fraction of vulnerable people of our society.

In the recent decades, academic research has been playing an important role in the identification, characterization and validation of new therapeutic targets against schistosomiasis²⁹. Different potential targets from *Schistosoma spp* have been described and have been widely studied: dihydroorotate dehydrogenase^{30; 31}, dihydrofolate reductase³²,

histone deacetylases³³, cathepsin B1³⁴, glutathione S-transferase³⁵, thioredoxin glutathione reductase³⁶, among others.

In this work, we want to bring up to discussion the relevance of exploiting the fumarases as potential drug targets against schistosomiasis.

1.3. Fumarate Hydratase

Fumarate hydratases (EC 4.2.1.2), or fumarases, are enzymes that catalyze the stereospecific and reversible hydration of fumarate to L-malate (**Figure 4**).

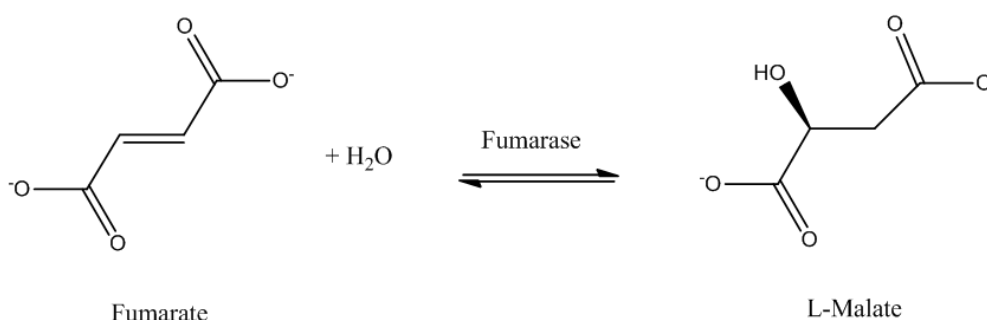


Figure 4. Reversible reaction catalyzed by fumarase enzyme.

The fumarases are classified in two distinct classes: class I fumarases (FH_IS) are homodimeric, contain an iron-sulfur cluster, and have a molecular weight around 120kDa^{37; 38; 39}, while class II fumarases (FH_{II}S) are homotetrameric, iron independent, have a molecular weight around 200kDa, and are characterized by a conserved amino acid signature (GSSxxPxKxNPxxxE) that contain the catalytic SS-loop sequence (**Figure 5**), common to all aspartase/fumarase superfamily members^{37; 38; 40; 41}.

Eukaryotic cells express two isoforms of fumarase^{42; 43}: the canonical role of fumarase is taken by the mitochondrial isoform that participates in the tricarboxylic acid (TCA) cycle and can also take part in the succinic fermentation pathways by providing fumarate for the enzyme fumarate reductase^{44; 45}; the cytosolic isoform has been described as having an important role in the maintenance of genome integrity. By migrating from the cytosol to the nucleus, the cytosolic FHs play a key role in DNA damage response (DDR) to DNA double strand breaks (DSBs)⁴⁶. Moreover, cytosolic fumarase was suggested to participate as a scavenger of fumarate from the urea cycle and catabolism of amino acids⁴⁷.

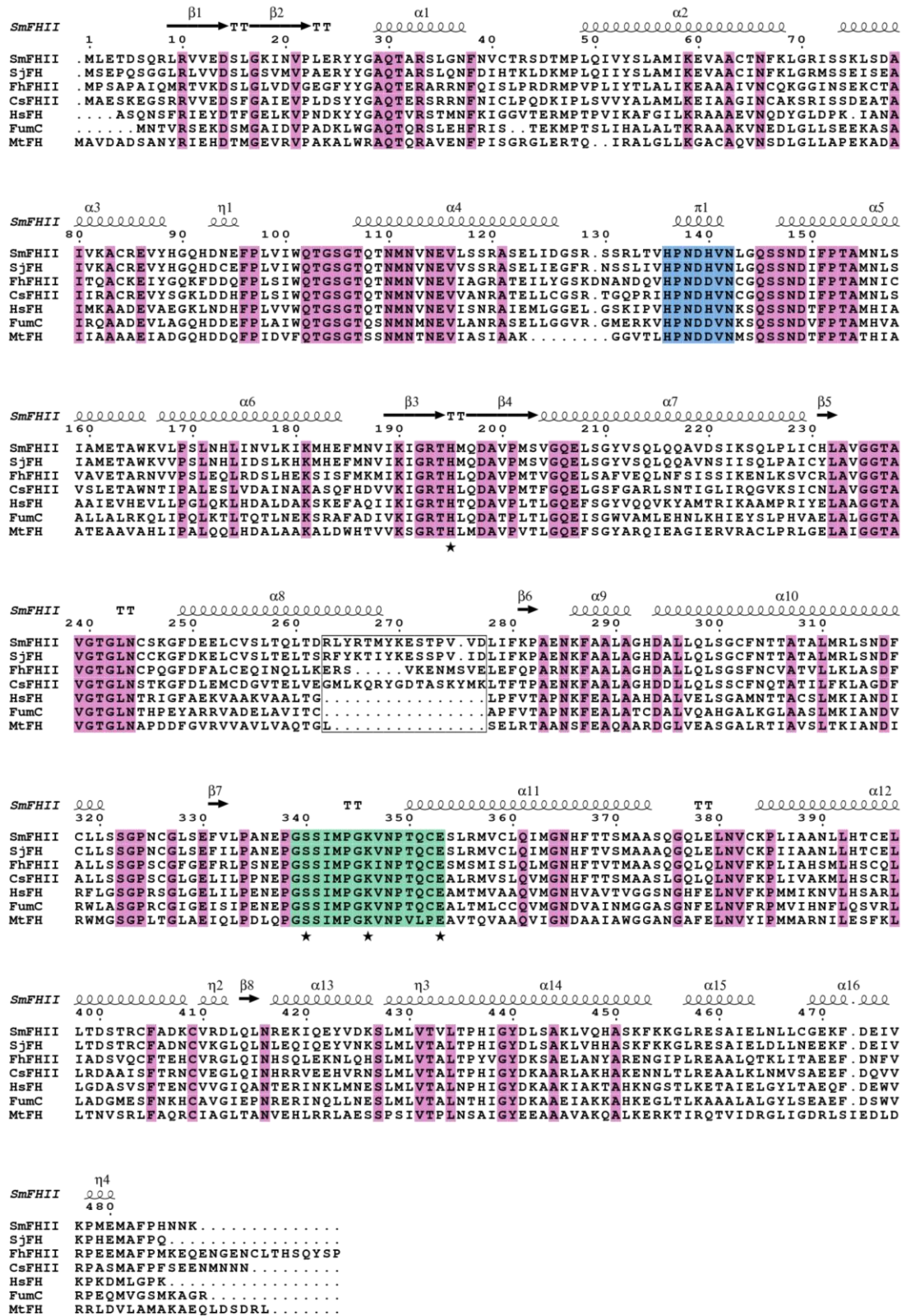


Figure 5. Sequence alignment of class II fumarases. SmFHII (*S. mansoni*), SjFH (*S. japonicum*), FhFHII (*Fasciola hepatica*), CsFHII (*Clonorchis sinensis*), HsFH (*Homo sapiens*), FumC (*Escherichia coli*), MtFH (*Mycobacterium tuberculosis*). The conserved residues are indicated in pink boxes. The conserved B site is indicated in blue boxes. The amino acid signature (GSSxxPxKxNPxxxE) is indicated in green box. The additional fragment is indicated by a dark line box. The catalytic residues are indicated by star symbols. The alignment was performed using MULTALIN and graphically displayed using ESPrpt⁴⁸.

Despite the functional relevance of fumarases, its reaction mechanism is not fully understood yet. The fumarate to L-malate conversion involves the hydration of fumarate by trans-1,4-addition of a hydroxyl group and a proton across the carbon-carbon double bond of fumarate resulting in the formation of L-malate. The reverse reaction proceeds with the elimination of a molecule of water from L-malate, generating fumarate⁴⁹.

The first class I fumarase three-dimensional structure was just described in 2016 for cytosolic *Leishmania major* fumarase (LmFH-2)³⁹. The LmFH-2 structure is distinct from class II fumarases, revealing a dimeric architecture that resembles a heart, with each lobe containing two domains that are arranged around the active site. Recently, the structure of mitochondrial *Leishmania major* fumarase (LmFH-1) was also solved, showing high structural similarity with LmFH-2⁵⁰.

Class II fumarases are known to share high structural similarity, having a tertiary and quaternary fold common to all aspartase/fumarase superfamily members. Each tetramer subunit has three domains: an N-terminal domain, a large central domain composed of 5 α -helices, and a C-terminal domain. The association of the four central domains in the tetramer forms a paired 20 α -helices core that is structurally rigid (**Figure 6**).

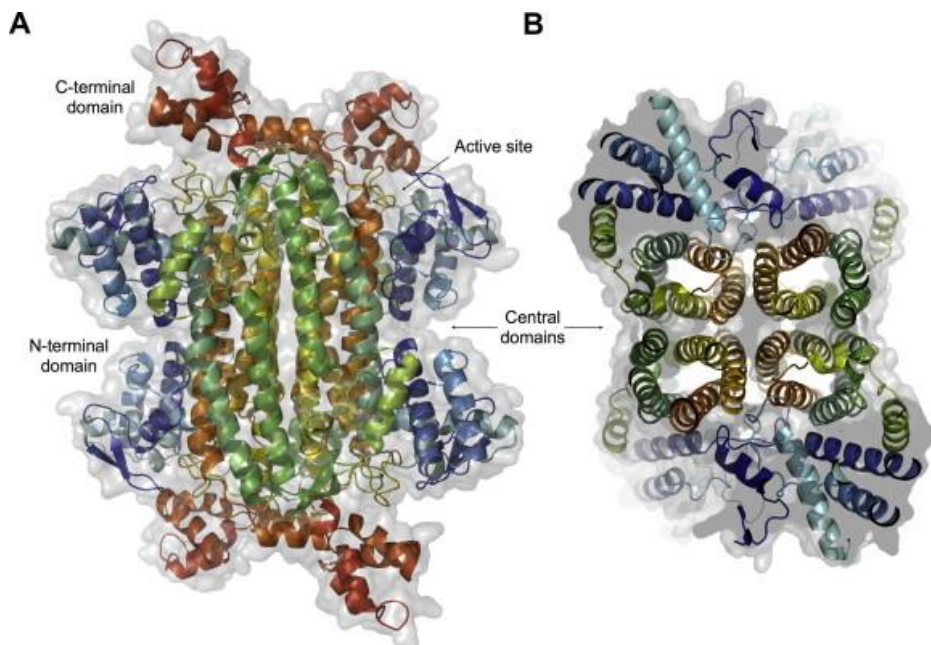


Figure 6. Fumarase structure encoded by Rv1098c *Mycobacterium tuberculosis* gene. The figure shows the central, N-terminal, and C-terminal domains in two different views. (Extracted from Mechaly, et al. 2012⁵¹).

The class II fumarases active site is composed by residues from three different chain regions, highly conserved among this class, and each region belongs to a distinct tetramer subunit. Thus, there are 4 active sites in the functional tetrameric enzyme.

1.3.1. Fumarase as a target to schistosomiasis

Fumarases are considered potential drug/therapeutic targets, since they are involved in important biological pathways. Recently, studies have been reported promising selective inhibitors to both classes: class II fumarases from *Mycobacterium tuberculosis*⁵², class I fumarases from *Leishmania major*⁵⁰, *Trypanosoma cruzi*⁵³ and *Plasmodium falciparum*⁵⁴.

Schistosoma mansoni, as well as other trematode worms, possesses the two classes of fumarases. Class I fumarase from *S. mansoni* (SmFH_I) is the mitochondrial enzyme and as such is predicted to contain an oxygen sensitive [4Fe-4S] cluster as a cofactor and to be involved in energy metabolism in *schistosoma spp.* Class II fumarase from *S. mansoni* (SmFH_{II}) is predicted to be the cytosolic enzyme responsible for metabolizing fumarate in the cytosol and when migrating to the nucleus may play an important role in maintaining genomic stability in the parasite.

Giving those distinct and relevant metabolic pathways in which SmFH_I and SmFH_{II} participates, we are interested in evaluating the inhibition of fumarase activity as a strategy to treat schistosomiasis.

Important to emphasize that since eukaryotes have the ability to shuttle malate and fumarate between mitochondria and cytosol, it is expected that the inhibition of only one isoform (SmFH_I or SmFH_{II}) would be inefficient to generate a complete deleterious effect on fumarase activity to the parasite. In fact, this hypothesis has been corroborated by different studies. For instance, fumarase knock out studies performed in *Trypanosoma cruzi* demonstrated that, although the cytosolic or mitochondrial fumarase activities are individually dispensable, their combined activity is essential for parasite viability⁵³. Moreover, studies using class II fumarase of *Bacillus subtilis* showed that when this single bacterial enzyme is expressed in a mutant yeast strain it can complement both TCA cycle and DDR eukaryotic functions.⁵⁵

Deeper comprehension of the relevance of fumarase activity in *Schistosoma spp.* will help us to fully understand the function of fumarases for the parasite and validate the

fumarases as drug targets to treat schistosomiasis. This work focused on the structural and kinetic characterization of *SmFH_{II}* and represents the very first step towards this goal.

2. OBJECTIVES

The aim of the present work was to perform structural, biochemical and biophysical characterization of the enzyme *Schistosoma mansoni* class II fumarate hydratase, as an important step towards drug target validation. For such studies, our proposal involves obtaining the enzyme in soluble form, functionally active, stable and with proper yield to perform the proposed studies. Thus, the following steps must be accomplished:

- Heterologous expression and purification of *SmFH_{II}* using *E. coli* as an expression system;
- Kinetic characterization and determination of optimum pH;
- Biophysical characterization by differential scanning fluorimetry and dynamic light scattering;
- Structural studies by X-ray crystallography.

3. MATERIALS AND METHODS

3.1. Gene cloning of *SmFH_{II}*

The codons in the open reading frame (Uniprot ID: G4LVG5) predicted for the putative class II *Schistosoma mansoni* fumarase were initially optimized for *E. coli* expression, and synthesized and cloned into a pUCminusMCS vector by Blue Heron® Biotech company. Due to errors in genome annotation, a 21 bp fragment was then removed using overlap extension polymerase chain reaction (**Figure 7**). The method consisted of two rounds of Polymerase Chain Reaction (PCR). Initially, PCR was performed using primers F1_f and F1_R, and primers F2_f and F2_R to amplify the first (fragment *a* comprising 1 to 1038) and second fragment (fragment *b* comprising 1060 to 1494), respectively. F1_f and F2_R have unique BamHI and XhoI restriction sites, respectively. The PCR mixture consisted of 0.4 mM of each primer, 0.2 mM dNTP mix, 2 mM MgCl₂, 1.25 U Phusion® HF DNA Polymerase, 1x Phusion® HF Buffer 10x and 200 ng DNA template in a 50 µL volume. The PCR was carried out using initial denaturation at 94 °C for 120 s, followed by 25 cycles of 30 s denaturation at 94 °C, annealing at 64 °C for 30 s and extension at 72 °C for 60 s, and a final extension step

of 10 min. The amplified fragments were excised from 1% agarose ethidium bromide containing gel and purified using Wizard® SV Gel and PCR CleanUp System.

In the second round the fragments *a* and *b* were then merged by PCR in a mixture consisted of 0.2 mM dNTP mix, 2 mM MgCl₂, 1.25 U Phusion® HF DNA Polymerase, 1x Phusion® HF Buffer 10x and the DNA template in a 50 µL volume. This PCR step was carried out in two parts: In the first round, denaturation at 94 °C for 120 s, followed by 5 cycles of 30 s denaturation at 94 °C, annealing at 64 °C for 30 s and extension at 72 °C for 60 s. The second round started with the addition of 0.4 mM of each primer (F1_f and F2_R) into the mixture, followed by a denaturation step at 94 °C for 120 s, 30 cycles of 30 s denaturation at 94 °C, annealing at 64 °C for 30 s and extension at 72 °C for 105 s. The reaction is concluded with a final extension step of 10 min. The amplified band corresponding to the expected *SmFH*_{II} gene size was excised from an agarose gel and purified as described above. The gene was digested with BamHI and XhoI restriction enzymes, and then ligated into a pET-28a(+)-sumo expression vector, previously digested with the same restriction enzymes, using T4 DNA ligase. The construct was designed to produce an N-terminal His6-sumo-tagged fusion protein.

Other construct was designed to express a protein, named *SmFH*_{II(Δ263-277)}, lacking an additional portion composed by 15 amino acid residues in *SmFH*_{II}. The region is also present in *S. japonicum* and other trematode worms, but is not present in the homolog human enzyme and other representative class II fumarases. The *SmFH*_{II(Δ263-277)} gene was also generated by overlap extension polymerase chain reaction using the *SmFH*_{II} gene construct as a template. Fragments *c* and *d* (**Figure 7**) were generated using primers F1_f and F3_R, and F3_f and F2_R respectively. The fragment containing the truncated *SmFH*_{II(Δ263-277)} enzyme was generated in a PCR reaction by combining fragments *c* and *d*, using the primers F1_f and F2_R. The final insert was then cloned into pET-28a(+)-sumo expression vector, using the same method described above. The success of the overlap extension PCR was then confirmed by nucleotide sequencing.

Table 1. Oligonucleotide primers used in overlap extension polymerase chain reaction.

Primer number	Sequence
F1 _f	GACGACGGATCCATGCTTGAAACTGA
F1 _R	GGTTGGGTAACTTTTCCTGGCATGATAGACGAGCCG
F2 _f	GTCTATCATGCCAGGAAAAGTTAACCCAACCCAATGTGAATCACTG
F2 _R	GTCTCGAGTCATTTGTTGTTGTGAGGAAAG
F3 _f	CTTGAAGATCAGATCAGTCAGTTGGGTAAG
F3 _R	AACTGACTGATCTGATCTTCAAGCCAGC

ATGCTTGAAACTGACTCCCAACGCCTGCGTGTAGTAGAAGATTCTCTCGGTAAAATCAATGTTCCGCTTGAACGCTACTATGG
 TGCACAAACTGCCCGCTCTTTAGGAAATTTTAAATGTTTGTACCCTTCCGATACCATGCCGCTCCAAATTGTCTATTCTCTCG
 CTATGATTAAAGAAGTTGCCGCTTGCACTAACTTTAAACTGGGTCGTATTTCTTCTAAATTGTCTGATGCCATTGTCAAAGCT
 TGCCGCGAAGTTTATCATGGTCAACACGATAATGAATTTCCACTTGTAACTGGCAAACCGGTTCCGGCACTCAAACCAATAT
 GAATGTAAATGAAGTACTCTCCTCCCGCGCTCTGAACTTATTGACGGCTCCCGTTCTCTCGTCTTACTGTCCATCCCAACG
 ACCATGTAAACCTGGGCCAGTCTCTAATGATATCTTTCCACTGCAATGAATCTTAGTATCGCCATGGAAACCGCTTGGAAA
 GTTCTGCCATCTTTAAATCATCTCATCAATGTACTGAAAATCAAATGCACGAATTTATGAATGTTATCAAATTTGGCCGTAC
 GCATATGCAAGACGCAGTCCCATGTCAGTTGGTCAGGAATTATCTGGTTACGTGAGCCAACCTCAACAAGCCGTCGATAGTA
 TTAAATCTCAACTCCCCCTCATCTGTCATCTCGCCGTTGGTGGAAACCGCTGTTGGTACTGGTCTGAACTGTTCTAAAGGTTTT
 GATGAAGAATTATGTGTTTCACTTACCCAAGTACTGATCGCCTGTATCGTACTATGTATAAAGAATCTACCCCGGTAGTAGA
 CTGATCTTCAAGCCAGCCGAAAATAAATTTGCCGCTCTCGCCGGTCATGATGCGCTTCTTCAGCTGTCTGGCTGCTTTAACA
 CTACTGCAACTGCGTTAATGCGTCTCTCTAACGACTTCTGCCTGTTATCTTCTGGCCCTAATTGCGGTCTTTTCAGAATTTGTG
 TTGCCTGCAAAATGAACCCGGCTCGTCTATCATGCCAGGAAAACTCTATCATACCTTCGGAAAAATTAACCAACCAATGTGA
 ATCACTGCGTATGGTATGCCTCCAAATTATGGGTAACCACTTTACTACCTCCATGGCGGCTAGTCAAGGCCAACCTGGAACTGA
 ATGTCTGTAAACCCCTGATCGCAGCCAACCTGTTGCATACTTGTGAGTTACTTACCGATTCTACCGTTGCTTCGCTGACAAA
 TGTGTGCGTGATCTTCAATTAAATCGCGAAAAAATCAAGAATATGTTGATAAATCCCTTATGTTGGTTACTGTTTAACTCC
 TCACATTGGTTACGACTTATCCGCAAACTGGTCCAACACGCGTCAAAATTTAAAAAAGGACTGCGCGAATCTGCTATTGAAT
 TGAATTTACTGTGCGGGGAAAAATTCGATGAGATTGTCAAACCATGGAAATGGCCTTTCTCACAACAACAAATGACTCGAG

Figure 7. Optimized codon of open reading frame for the putative class II *Schistosoma mansoni* fumarase based on the sequence available in GenBank (Uniprot ID: G4LVG5). Overlap extension PCR was used to remove error in gene annotation (red). Fragments a (blue) and b (pink) were combined creating the construct *SmFH_{II}*, consisting of the pET-28a(+)-sumo vector and a 1473 bp gene fragment. For functional studies the region highlighted in yellow was removed. Fragments c (green) and d (purple) were used for overlap extension PCR creating the construct named *SmFH_{II}(Δ 263-277)* consisting of the pET-28a(+)-sumo vector and a 1428 bp gene fragment.

3.2. Protein expression and purification

In order to express both *SmFH_{II}* and *SmFH_{II}(Δ 263-277)* enzymes, *Escherichia coli* BL21(DE3) were initially transformed with the plasmids *SmFH_{II}*-pET-28a(+)-sumo and *SmFH_{II}(Δ 263-277)*-pET-28a(+)-sumo. Cells from a single colony were grown in 10 mL of LB media overnight at 37°C and used to inoculate 1 L of LB media containing 30 µg/mL kanamycin. Expression was induced when the culture reached an OD₆₀₀ of 0.6 by adding 0.5 mM isopropyl β-D-1-thiogalactopyranoside - IPTG, and the culture was continued to grow for further 20 h, at 18°C. The cells were then harvested by centrifugation (8,000 *xg*) at 4°C and stored at -20°C.

The pelleted cells were resuspended in 30 mL of lysis buffer (50 mM NaH₂PO₄ pH 8.5, 300 mM sodium chloride, and 1 mM phenylmethylsulfonyl fluoride - (PMSF)). The cells were lysed by sonication at 4°C, in a Misonix XL 2000 sonicator, and the cell lysate was clarified by centrifugation (16,000 *xg*) for 30 min at 4°C. The soluble fraction was applied into a 2 mL of Ni-NTA agarose resin packed in a Poly-Prep column that had been pre-equilibrated with initial buffer (50 mM NaH₂PO₄ pH 8.5, 300 mM NaCl). To eliminate contaminants, the resin was washed with 20mL of the initial buffer followed by 20 mL of buffer containing 25mM imidazole (50 mM NaH₂PO₄ pH 8.5, 300 mM NaCl, and 25 mM imidazole). The column was then re-equilibrated with 10 mM imidazole buffer (50 mM NaH₂PO₄ pH 8.5, 300 mM NaCl, and 10 mM imidazole), and the N-terminal His6-tagged SUMO portion was removed by addition of ULP1 (Ubiquitin-like-specific Protease 1 - EC 3.4.22.68). Cleavage was performed at 4°C, during 4h, and tag-free *SmFH_{II}* was then eluted using 20 mL of 10 mM imidazole buffer (50 mM NaH₂PO₄ pH 8.5, 300 mM NaCl, and 10mM imidazole). His6-sumo-tagged portion and ULP1 protein were eluted by washing the column with 500 mM imidazole buffer (50 mM NaH₂PO₄ pH 8.5, 300 mM NaCl, and 500 mM imidazole). In the case of *SmFH_{II}(Δ 263-277)*, 10% glycerol was added to all buffers. To confirm the efficiency of recovery, the fractions of all purification steps were visualized using 14% SDS-PAGE.

Protein concentration was calculated using the theoretical molar extinction coefficient at 280 nm estimated by the ExPASy ProtParam tool ($\epsilon_{280\text{nm}} = 101640 \text{ M}^{-1} \cdot \text{cm}^{-1}$ for *SmFH_{II}* and $\epsilon_{280\text{nm}} = 89720 \text{ M}^{-1} \cdot \text{cm}^{-1}$ for *SmFH_{II}(Δ 263-277)*).

3.3. Size exclusion chromatography and DLS experiments

Size exclusion chromatography was performed in an Äkta Purifier system (GE Healthcare Life Science®), using a Superdex 200 (10/300) GL column (GE Healthcare Life Science®) pre-equilibrated with 50 mM Tris-HCl pH 8.5 and 150 mM NaCl (or the same buffer containing 10% glycerol, in the case of *SmFH_{II}(Δ 263-277)*) at flow rate of 0.5 mL/min. Protein elution was monitored at 280nm. The Superdex column was previously calibrated with separated runs of the protein molecular weight markers (ribonuclease (13,7 kDa), carbonic anhydrase (29 kDa), conalbumin (75 kDa), aldolase (158 kDa), ferritin (440 kDa)). Blue Dextran 2000 was used to measure the void volume of the column. The standards were run separately. For *SmFH_{II}* and *SmFH_{II}(Δ 263-277)* characterization, fractions eluted from affinity column were pooled, concentrated by AMICON 30 kDa (Millipore) and analyzed with the same Superdex 200 gel filtration column.

Dynamic light scattering (DLS) was performed in a Zetasizer Nano ZS (Malvern Instruments) at 18 °C, with a volume of 50 μ L in a quartz cuvette ZEN2112. The protein sample was prepared at a final concentration of 10 mg/mL, and was previously centrifuged for 10 min at 15,800 xg . Data analysis was performed using the Zetasizer software.

3.4. Differential Scanning Fluorimetry

Differential Scanning Fluorimetry experiments were carried out in a thermocycler Mx3005P (Agilent Technologies), using SYPRO® orange (492/610 nm) as a fluorescent probe in a 96-well PCR plate. The behavior of *SmFH_{II}* and *SmFH_{II}(Δ 263-277)* in the presence of different chemical environments was analyzed using the Solubility & Stability Screen (Hampton Research). The 20 μ L reaction mixture contained 75 μ g/mL of protein and 5X SYPRO® orange. Variation in pH and ionic strengths were assayed using Solubility & Stability Screen 2 (Hampton Research). In addition, 50 mM sodium acetate at pHs 5 and 5.5 were also tested in presence of increasing concentrations of NaCl (0; 50; 100; 150; 200; 250; 500 and 1000 mM). The 20 μ L reaction mixture contained 100 μ g/mL of protein and 5X SYPRO® orange. The samples were heated from 25 to 95 °C at 1 °C/min and fluorescence measurements were taken. Thermal melting curves were processed according to the protocol described by Niesen et al⁵⁶, and the melting temperature was calculated using GraphPad Prism software.

3.5. Kinetics assay

SmFH_{II} and *SmFH_{II}(Δ263-277)* activity was assayed by monitoring the production or consumption of fumarate in a Spectra Max Plus 384 Microplate Reader (Molecular devices), at room temperature, and all readouts were made in three replicates. The concentration of the fumarate was estimated at 250 nm ($\epsilon_{250\text{nm}} = 1.45 \text{ mM}^{-1} \cdot \text{cm}^{-1}$) for solutions that contained L-malate or fumarate concentrations up to 1 mM, and at 272nm ($\epsilon_{272\text{nm}} = 0.48 \text{ mM}^{-1} \cdot \text{cm}^{-1}$) for high concentrations of fumarate. To determine the optimum pH for enzyme activity, a single point assay was performed under a broad range of pHs (50mM MES pH 6 and 6.5; 50 mM HEPES pH 7 and pH7.5; 50 mM Tris pH8, pH 8.5 and pH 9; all of them containing 150 mM KCl and 10 mM L-malate or 0.5 mM fumarate), in a total volume of 200 μL . The reaction was started by adding the enzyme at the final concentration of 100 nM, and the measurement was monitored for 60 s. To determine the steady-state kinetics parameters, an enzymatic kinetic assay was set using both substrates (fumarate and L-malate), simultaneously. The activity buffer was composed by 50 mM Tris pH 7.5, 150 mM KCl and L-malate (0.039, 0.078, 0.156, 0.312, 0.625, 1.25, 2.5, 5, 10, and 20 mM) and fumarate (0.007, 0.015, 0.031, 0.062, 0.125, 0.25, 0.5, 1 and 2 mM).

The kinetics constants were estimated using the equation for reversible kinetics given below:

$$\frac{v}{[E]} = \frac{k_{\text{cat}}^{\text{f}}[\text{MAL}]}{K_{\text{m}}^{\text{MAL}}\left(1 + \frac{[\text{FUM}]}{K_{\text{m}}^{\text{FUM}}}\right) + [\text{MAL}]} - \frac{k_{\text{cat}}^{\text{r}}[\text{FUM}]}{K_{\text{m}}^{\text{FUM}}\left(1 + \frac{[\text{MAL}]}{K_{\text{m}}^{\text{MAL}}}\right) + [\text{FUM}]} \quad \text{Equation 1}$$

where [FUM] and [MAL] correspond to concentrations of each substrate, [E] correspond to enzyme concentration, $K_{\text{m}}^{\text{FUM}}$ and $K_{\text{m}}^{\text{MAL}}$ are the Michaelis-Menten constants to fumarate and L-malate, respectively, $k_{\text{cat}}^{\text{f}}$ is the catalytic constant for the conversion of L-malate into fumarate, $k_{\text{cat}}^{\text{r}}$ is the catalytic constant for the conversion of fumarate into L-malate, and v is the global velocity of the reaction.

Data were processed and analyzed using the programs OriginPro 8 (OriginLab) and Sigmaplot (Systat Software).

For comparison, the human enzyme was produced as previously described⁵⁷, purified under the same conditions of *SmFH_{II}*, and its kinetics constants estimated as described above.

3.6. X-ray crystallography

Crystallization experiments were performed using the vapor diffusion techniques, by sitting drop method^{58; 59}. 1 μ L of protein solution (10 mg/mL in 50 mM Tris-HCl pH 8.5, 150 mM NaCl) was mixed with 1 μ L of reservoir solution, and equilibrated against 500 μ l of reservoir solution at 21°C. The crystallization experiments of *SmFH_{II}* were performed by screening the commercial kits: Crystal Screen 1 and 2, PEG Ion 1 and 2, PEGRx 1 and 2, Index HT, SaltRx HT and Natrix HT (Hampton Research). After 3 days, needle crystals were obtained in condition 91 of Index HT (Hampton Research), containing 150 mM malate pH7 e 20% PEG 3350. The hit condition was then optimized by screening pH, precipitant concentration, protein concentration and also using microseeding techniques⁶⁰. Once *SmFH_{II}* crystals were obtained, they were soaked in a cryoprotectant solution (100 mM sodium acetate pH 4, 100 mM malate, 14% PEG 3350, and 25% glycerol), harvested with cryo loops, and were flash-cooled in liquid nitrogen. The data set was collected at 100 K on a synchrotron facility (PROXIMA 2 - SOLEIL, France) using a PILATUS 6M detector (Dectris, Baden, Switzerland). The images of x-ray diffraction were processed and scaled with XDS⁶¹ package, and the structure of *SmFH_{II}* was solved by molecular replacement implemented in Molrep program⁶², using the human fumarase structure (PDB ID: 5D6B)⁵⁷ as template. Automated model rebuilding was performed using Buccaneer⁶³, and the structure was refined with Refmac⁵⁶⁴ intercepted with manual map inspection and model building using Coot⁶⁵.

4. RESULTS

4.1. *SmFH_{II}* production and oligomeric characterization

The open reading frame predicted to encode the cytosolic fumarase class II from *Schistosoma mansoni* was initially synthesized based on the coding sequence deposited in GenBank (Uniprot ID: G4LVG5). The resultant protein was found to contain a 7 amino acids long insertion located within the class II fumarase signature (**Figure 8**). Studies performed in our laboratory demonstrated that the product of this gene lacked fumarase activity (results not shown), suggesting an error in gene annotation. Homology modeling studies predicted the correct coding sequence for *SmFH_{II}*, which was later confirmed by more recent data deposited

in different gene databases, such as the WormBase ParaSite (Smp_158240.2). The synthetic gene was then used as a template for removal of the incorrect 21 base pairs fragment.

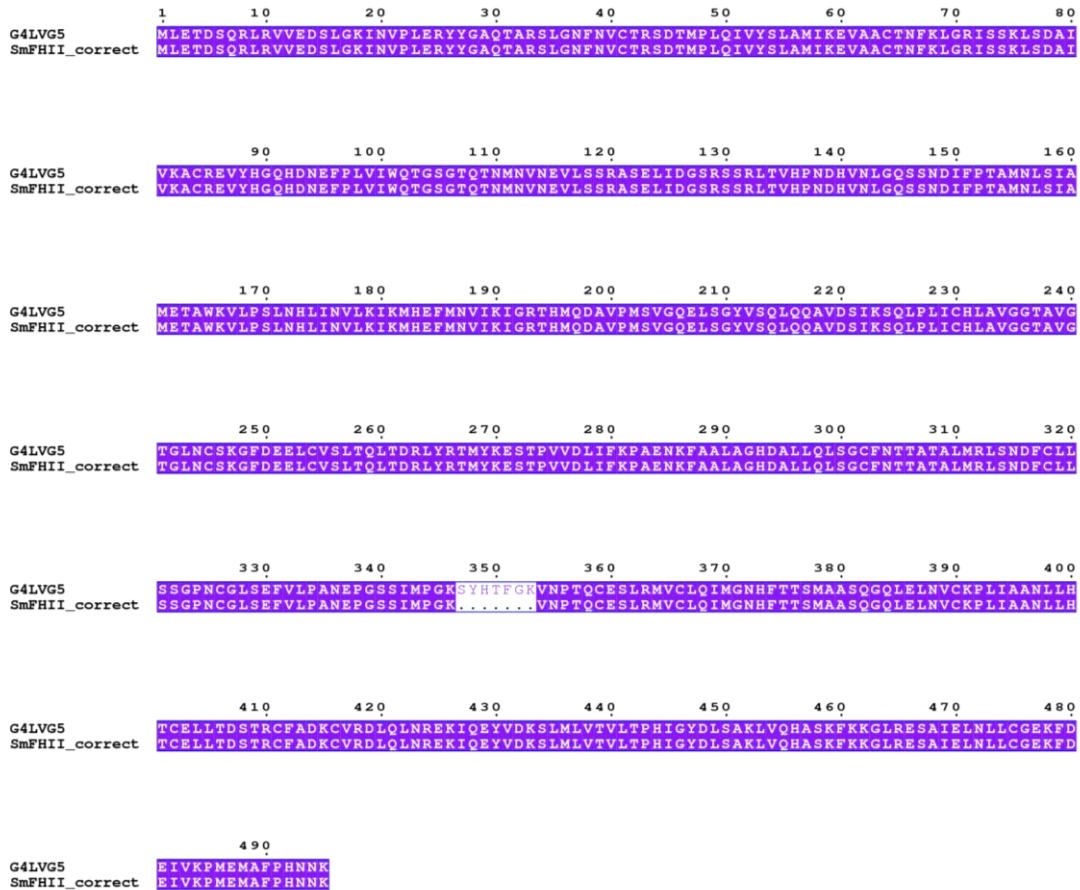


Figure 8. Alignment between the predicted protein (Uniprot ID G4LVG5) and the correct amino acid sequence of class II fumarate hydratase from *S. mansoni* (SmFHII_correct).

Full length *SmFHII* was expressed in *E. coli* BL21 (DE3) as a soluble protein and purified to homogeneity, with a yield of approximately 14 mg of active recombinant protein per liter of culture (**Figure 9**).

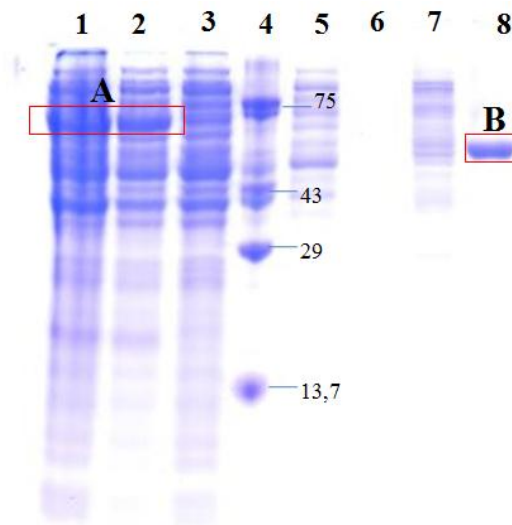


Figure 9. 14% SDS-PAGE representing all steps of *SmFH_{II}* purification using an affinity column (Ni-NTA agarose resin): (1) Pellet; (2) Supernatant; (3) Ni-NTA affinity column flow through; (4) Protein molecular weight marker (kDa); (5) Column wash with 0 mM imidazole; (6) Empty well (7) Column wash with 25 mM imidazole; (8) *SmFH_{II}* elution after cleavage with ULP1. “A” highlight the band corresponding to enzyme with tag. “B” highlight the band corresponding to purified enzyme without the tag.

In order to probe the oligomeric state of pure recombinant *SmFH_{II}*, both size exclusion chromatography (SEC) and dynamic light scattering (DLS) techniques were carried out. Estimation of the *SmFH_{II}* average molar mass was performed by relating the elution volume to the respective molar mass estimated from the calibration curve (**Figure 11**). The active enzyme eluted at a volume of 12.98 ml, corresponding to the molecular mass of a tetramer (209 kDa). DLS experiments show that the purified protein sample is homogenous, monodisperse, and that presents the expected radii for the tetrameric form (**Figure 12A**), in agreement with the studies performed by size exclusion chromatography and compatible with the expected oligomeric state reported for class II fumarases.

When compared to other representative class II fumarases, *SmFH_{II}* presents a 15 residues insert sequence, comprising the amino acids 263 to 277 (**Figure 5**). In order to evaluate the relevance of this portion in the *SmFH_{II}* structure and catalysis, we designed a new construct, named *SmFH_{II}(Δ 263-277)*, that lacks this additional sequence.

SmFH_{II}(Δ 263-277) was initially expressed and purified under the same experimental conditions as *SmFH_{II}*, with a yield of 6 mg per liter of culture (**Figure 10**). In the size exclusion chromatography, *SmFH_{II}(Δ 263-277)* eluted at the volume of 13.01 ml, which also corresponds to the molecular mass of a tetramer (206 kDa) (**Figure 11**). The increase in both

polydispersity and average size observed in our preliminary DLS experiment suggested stability issues for *SmFH_{II}(Δ 263-277)* enzyme in solution (**Figure 12B**). Protein aggregation and heterogeneity were prevented by adding 10% glycerol in all buffers throughout purification (**Figure 12C**).

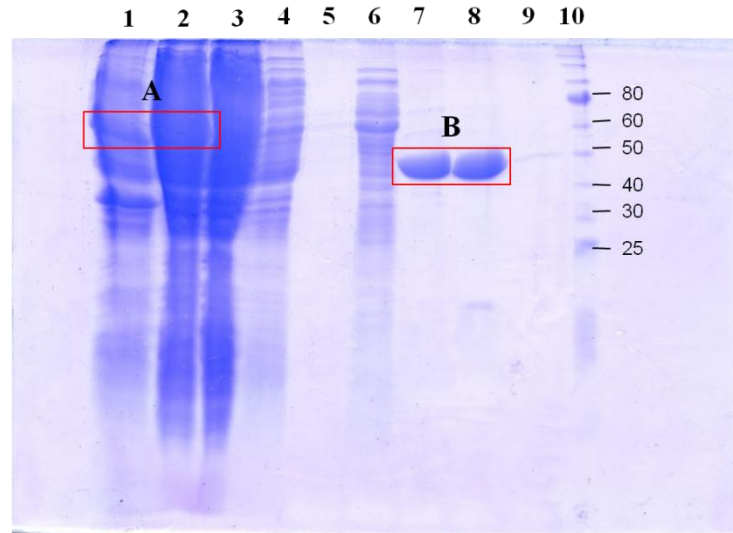


Figure 10. 14% SDS-PAGE representing all steps of *SmFH_{II}(Δ 263-277)* purification using an affinity column (Ni-NTA agarose resin): (1) Pellet; (2) Supernatant; (3) Ni-NTA affinity column flow through; (4) Column wash with 0 mM imidazole; (5) Empty well (6) Column wash with 25 mM imidazole; (7) and (8) *SmFH_{II}(Δ 263-277)* elution after cleavage with ULP1; (9) Empty well (10) Protein molecular weight marker (kDa). “A” highlight the band corresponding to enzyme with tag. “B” highlight the band corresponding to purified enzyme without the tag.

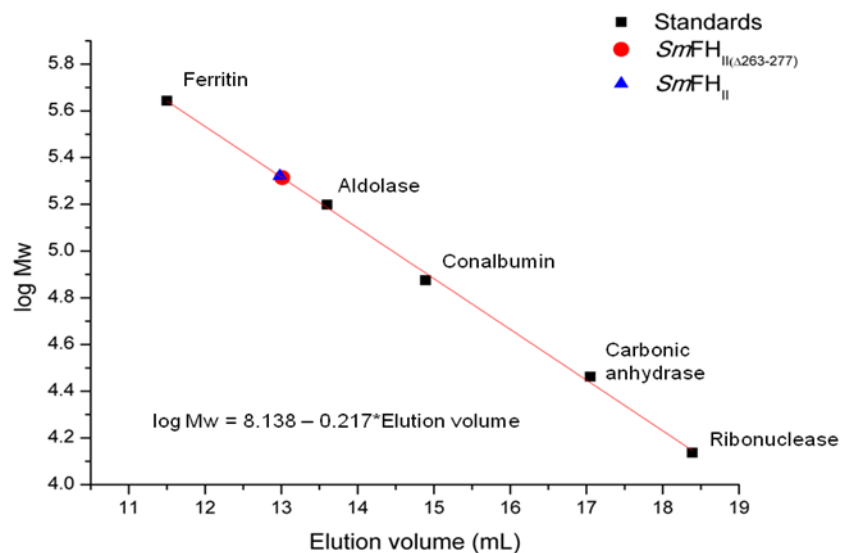


Figure 11. Oligomeric state determination of recombinant *SmFH_{II}* and *SmFH_{II}(Δ 263-277)* by gel filtration. The molecular mass standards used were ferritin (440 kDa), aldolase (158 kDa), conalbumin (75 kDa), carbonic anhydrase (29 kDa), and ribonuclease (13.7 kDa). The elution volume under non-denaturing conditions for *SmFH_{II}* (12.98 mL) and *SmFH_{II}(Δ 263-277)* (13.01 mL) is indicated, demonstrating the enzymes to be a homotetramer.

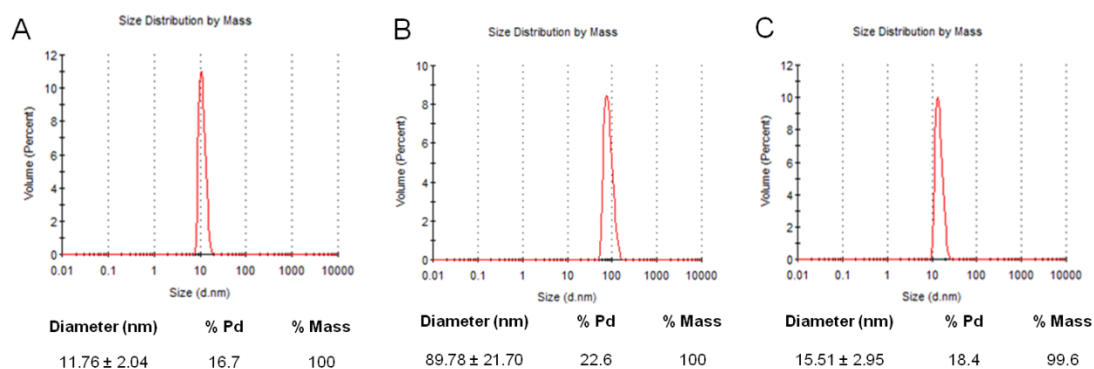


Figure 12. Mass distribution of light scattered by protein solution as a function of particle diameter. (A) *SmFH_{II}* in buffer (50 mM Tris-HCl pH 8.5 and 150 mM NaCl); (B) *SmFH_{II}(Δ 263-277)*: in buffer; (C) *SmFH_{II}(Δ 263-277)* in buffer added 10% glycerol.

4.2. DSF analysis

DSF was used to map the response of both *SmFH_{II}* and *SmFH_{II}(Δ 263-277)* to different physicochemical environments. Reference (water) melting temperature (T_m) for *SmFH_{II}* was $49.08\text{ }^\circ\text{C} \pm 0.03$, whereas for *SmFH_{II}(Δ 263-277)* was $31.73\text{ }^\circ\text{C} \pm 0.09$. Melting curves revealed a significant gain in thermal stability for both *SmFH_{II}* and *SmFH_{II}(Δ 263-277)* when in presence of compounds that have been previously reported as fumarase inhibitors⁶⁶ (**Table S1 and S2**): succinic acid ($\Delta T_m = 10.27\text{ }^\circ\text{C}$ and $11.84\text{ }^\circ\text{C}$), sodium malonate ($\Delta T_m = 9.41\text{ }^\circ\text{C}$ and $5.30\text{ }^\circ\text{C}$), DL-malic acid ($\Delta T_m = 11.12\text{ }^\circ\text{C}$ and $16.74\text{ }^\circ\text{C}$), tacsimate ($\Delta T_m = 8.97\text{ }^\circ\text{C}$ and $9.59\text{ }^\circ\text{C}$), glycine ($\Delta T_m = 10.02\text{ }^\circ\text{C}$ and $9.74\text{ }^\circ\text{C}$) and phosphate ($\Delta T_m = 12.24\text{ }^\circ\text{C}$ and $19.65\text{ }^\circ\text{C}$).

Protein thermal stability versus pH follows a normal distribution. For *SmFH_{II}* the highest thermal stability can be reached around pH 7.5, while for *SmFH_{II}(Δ 263-277)* maximum thermal stability is achieved around pH 6.5. In both cases, protein stability was found to increase with increasing salt concentration (**Figure 13A and 13C**).

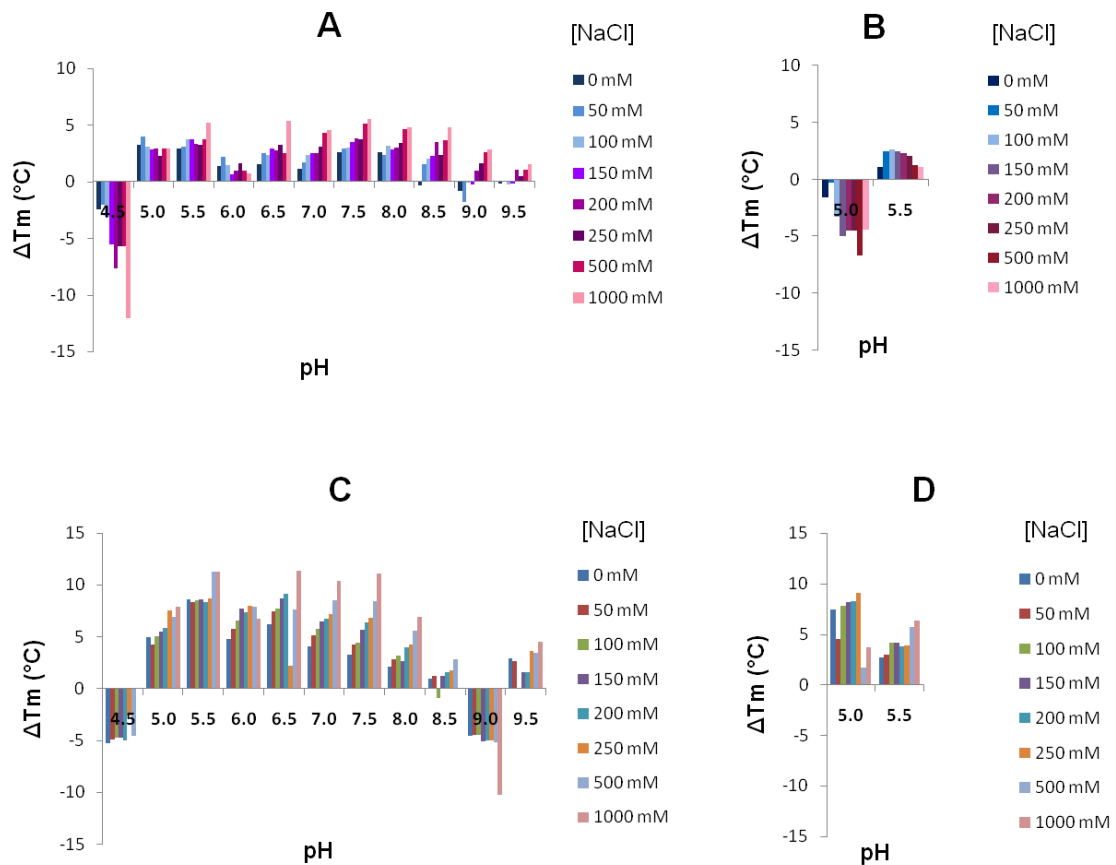


Figure 13. Thermostability assay for *SmFH_{II}* and *SmFH_{II}(Δ 263-277)* comparing pH versus salt concentration. **A** and **B** - *SmFH_{II}*; **C** and **D** - *SmFH_{II}(Δ 263-277)*. Buffers composition: **A** and **C** (pH 4.5 is 50 mM Sodium acetate trihydrate; pH 5.0 is 50 mM Sodium citrate; pH 5.5 is 50 mM Sodium succinate; pH 6.0 is 50 mM MES monohydrate; pH 6.5 is 50 mM BIS-TRIS; pH 7.0 is 50 mM Imidazole; pH 7.5 is 50 mM HEPES; pH 8.0 is 50 mM Tris; pH 8.5 is 50 mM BIS-TRIS Propane; pH 9.0 is 50 mM AMPD and pH 9.5 is 50 mM Glycine) **B** and **C** (50 mM Sodium acetate trihydrate).

As observed for human fumarase⁶⁷, an unusual thermal stability was also observed at the acidic pHs 5 and 5.5 (**Figure 13A and 13C**). This effect is due to the chemical nature of the buffers (citrate pH 5 and succinate pH 5.5) which are structurally related to *SmFH_{II}* substrates and were previously reported as competitive inhibitors of fumarases^{68; 69}. Similarly to what it has been done for the human homologue enzyme, thermostability of both *SmFH_{II}* and *SmFH_{II}(Δ 263-277)* were also tested in presence sodium acetate at pHs 5 and 5.5 (**Figure 13B and 13D**). However, unlike the human enzyme, at pH 5.5, acetate was found to induce a positive thermoshift for both constructs, in particular for *SmFH_{II}(Δ 263-277)*, that also had a great thermal stabilization in sodium acetate pH 5 (**Figure 13B and 13D**).

4.3. Optimum pH and kinetics assay

To determine the optimum pH for both $SmFH_{II}$ and $SmFH_{II(\Delta 263-277)}$ enzymes, a single point assay was performed under a broad range of buffers. Results were found very similar for both constructs. For fumarate, optimum pH was found to lay around 7-7.5 (**Figure 14**), whereas for L-malate, optimum pH was found around pH 8.

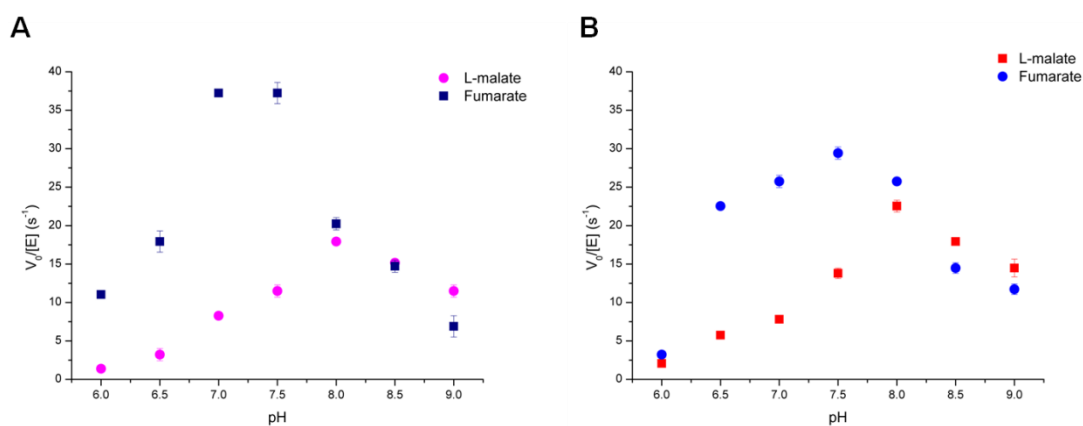


Figure 14. Enzyme activity measured as a function of pH. Optimum pH assay performed at single concentrations of substrates (10 mM L-malate or 0.5 mM fumarate). Effect of pH on reaction rate of (A) $SmFH_{II}$ and (B) $SmFH_{II(\Delta 263-277)}$.

As a strategy to evaluate and quantify the contribution of the reverse reaction in the determination of the steady-state kinetic parameters, the assay was performed with both substrates (fumarate and L-malate), simultaneously. The resultant surface curve (**Figure 15**) was fitted into the model of reversible reaction (Equation 1) and the steady-state parameters were determined (**Table 1**).

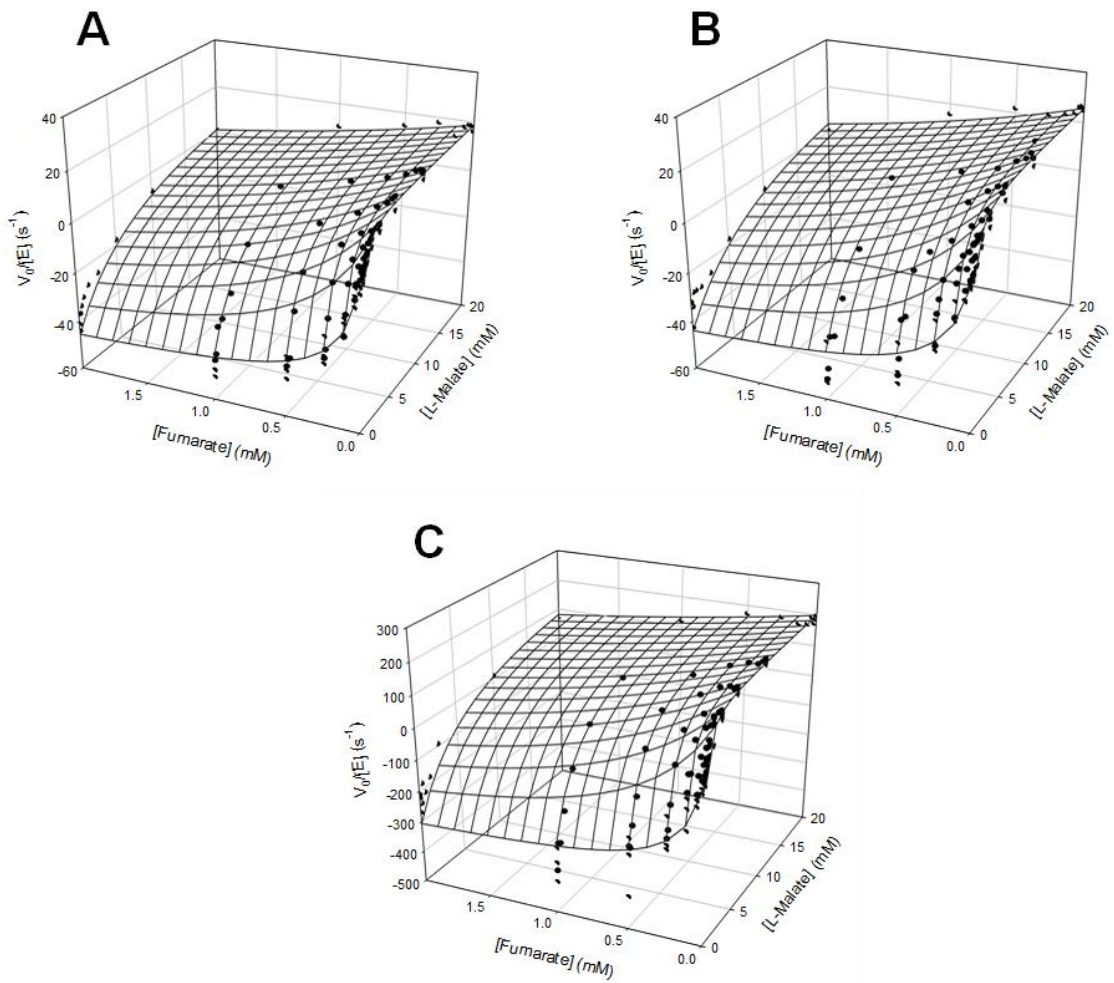


Figure 15. Surface graph of complete steady-state kinetics of *SmFH_{II}* (A), *SmFH_{II}(Δ263-277)* (B) and *HsFH* (C) with both substrates (L-malate and fumarate) simultaneously.

Table 2. Kinetics parameters* obtained in the steady-state kinetic with both substrates (L-malate and fumarate).

<i>SmFH_{II}</i>		<i>SmFH_{II}(Δ263-277)</i>		<i>HsFH</i>	
k_{cat}^f (s ⁻¹)	19 ± 1	k_{cat}^f (s ⁻¹)	26 ± 1	k_{cat}^f (s ⁻¹)	200 ± 10
K_m^{MAL} (mM)	0.56 ± 0.08	K_m^{MAL} (mM)	0.9 ± 0.2	K_m^{MAL} (mM)	0.52 ± 0.09
$\frac{k_{cat}^f}{K_m^{MAL}}$ (mM ⁻¹ s ⁻¹)	34 ± 7	$\frac{k_{cat}^f}{K_m^{MAL}}$ (mM ⁻¹ s ⁻¹)	29 ± 6	$\frac{k_{cat}^f}{K_m^{MAL}}$ (mM ⁻¹ s ⁻¹)	390 ± 90
k_{cat}^r (s ⁻¹)	49 ± 2	k_{cat}^r (s ⁻¹)	48 ± 2	k_{cat}^r (s ⁻¹)	330 ± 20
K_m^{FUM} (mM)	0.15 ± 0.02	K_m^{FUM} (mM)	0.20 ± 0.03	K_m^{FUM} (mM)	0.18 ± 0.03
$\frac{k_{cat}^r}{K_m^{FUM}}$ (mM ⁻¹ s ⁻¹)	330 ± 20	$\frac{k_{cat}^r}{K_m^{FUM}}$ (mM ⁻¹ s ⁻¹)	240 ± 50	$\frac{k_{cat}^r}{K_m^{FUM}}$ (mM ⁻¹ s ⁻¹)	1900 ± 400

* K_m^{FUM} and K_m^{MAL} are the Michaelis-Menten constants to fumarate and L-malate, respectively; k_{cat}^f is the catalytic constant for the conversion of L-malate into fumarate, k_{cat}^r is the catalytic constant for the conversion of fumarate into L-malate.

Comparison with the results obtained for the human enzyme (*HsFH*) under the same experimental conditions (**Table 1**) shows that parasitic and human enzymes share similar K_m values. On the other hand, k_{cat} values are almost 7-10 times higher for *HsFH*. As previously described for human fumarase, the catalytic efficiency for fumarate is higher than for L-malate, indicating that the reaction favors the formation of L-malate.

4.4. Overall structure of *SmFH_{II}*

Needle-shaped crystals were identified during the initial screening stage (**Figure 16A**). Optimization of pH, precipitant and additive concentrations and the use of microseeding techniques were successfully applied in order to improve external crystal morphology. Diffraction-quality crystals were obtained in the presence of 100 mM malate, 100 mM sodium acetate pH 4, and 12% polyethylene glycol 3350 (**Figure 16B**). The best data set obtained was processed at 1.85 Å of resolution. *SmFH_{II}* crystals belong to monoclinic space group C2, with cell unit parameters $a=180.65$, $b=67.86$ and $c=187.27$ Å; $\beta=118.61$. The structure of *SmFH_{II}* was determined by molecular replacement techniques using the human fumarase structure (PDB ID: 5D6B)⁵⁷ as the search model.

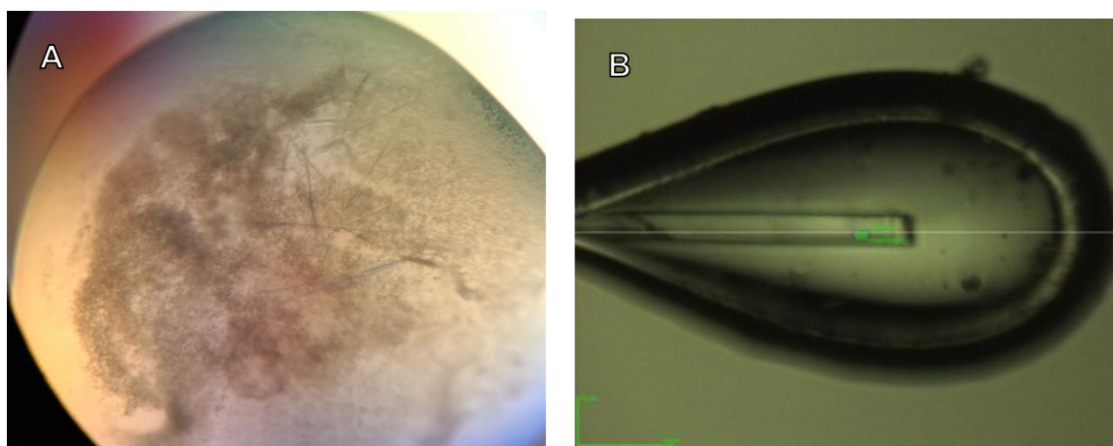


Figure 16. *SmFH_{II}* crystals. **A** - Crystals obtained during the initial screenings. **B** - Crystal from the optimized crystallization condition, used for the data collection.

The asymmetric unit contains two independent dimers. Each dimer forms the expected functional tetramer by crystallographic two fold symmetry axis (**Figure 17C**). The chain A comprises residues from 8 to 486, chain B from 9 to 486, chain C from 9 to 485 and chain D from 8 to 485. Residues missing from the expected polypeptide chain were excluded from the model due to the lack of interpretable electronic density and 893 solvent sites were treated as water oxygens. There are four molecules of L-malate, one at each active site, and 4 molecules of acetate, one at each chain. Interesting, there are 2 molecules of glycerol in chain A, 1 in chain B, 1 in chain C, and none in chain D, and it is possibly due to the crystal packing. The final round of refinement reached R_{work} of 0.192 and R_{free} of 0.227. Final refinement and geometry statistics are given in **Table 3**. The final structure and respective coordinates and structure factors were deposited in the Protein Data Bank (PDB) with the accession code 6U4O.

Table 3. Data collection and refinement statistics.

<i>Data collection</i>	
Beamline	Proxima 2 (SOLEIL)
Space group	C2
Cell dimensions	
a, b, c (Å)	180.65, 67.86, 187.27
α, β, γ (°)	90, 118.61, 90
Resolution range (Å)	46.93 - 1.85 (1.90 - 1.85)
CC1/2	99.7 % (55.2 %)
$I/\sigma(I)$	11.2 (1.1)
Completeness (%)	98.6 % (88.4%)
Multiplicity	6.8 (6.2)
<i>Refinement</i>	
Resolution (Å)	1.85
No. reflections	167349
$R_{\text{work}}/R_{\text{free}}$	0.192/0.227
Total number of atoms	29877
Average B -factors, all atoms (Å ²)	32.0
R.m.s. deviations	
<i>Bond lengths</i> (Å)	0.0054

<i>Bond angles (°)</i>	1.345
------------------------	-------

Statistics for the highest-resolution shell are shown in parentheses.

Each *SmFH_{II}* chain can be described as being composed of three domains: D1 (residue 8 to 144), D2 (residue 145 to 416) and D3 (residue 417 to 486), being very similar to other class II fumarases^{51; 70} (**Figure 17A, Figure 5**). D1 contains α -helices (α 1–4), 3_{10} -helix (η 1), π -helix (π 1) and strands (β 1–2), D2 contains α -helices (α 5–12), 3_{10} -helix (η 2), and strands (β 3–4) and D3 contains α -helices (α 13–16) and 3_{10} -helices (η 3–4) (**Figure 17B**). Packing of D2 domains from the different chains results in the assemble of 20 paired α -helices in the functional tetramer (**Figure 17C**). The additional portion composed of 15 residues in *SmFH_{II}* structure, removed in *SmFH_{II} Δ 263-277* construct, was revealed to partially fold as continuation of the α -helix 8 (residues from 263 to 277) in the central domain (D2) (**Figure 18A**). This portion was found as a protuberant and solvent exposed region, and is characterized by the presence of polar residues (**Figure 18B**).

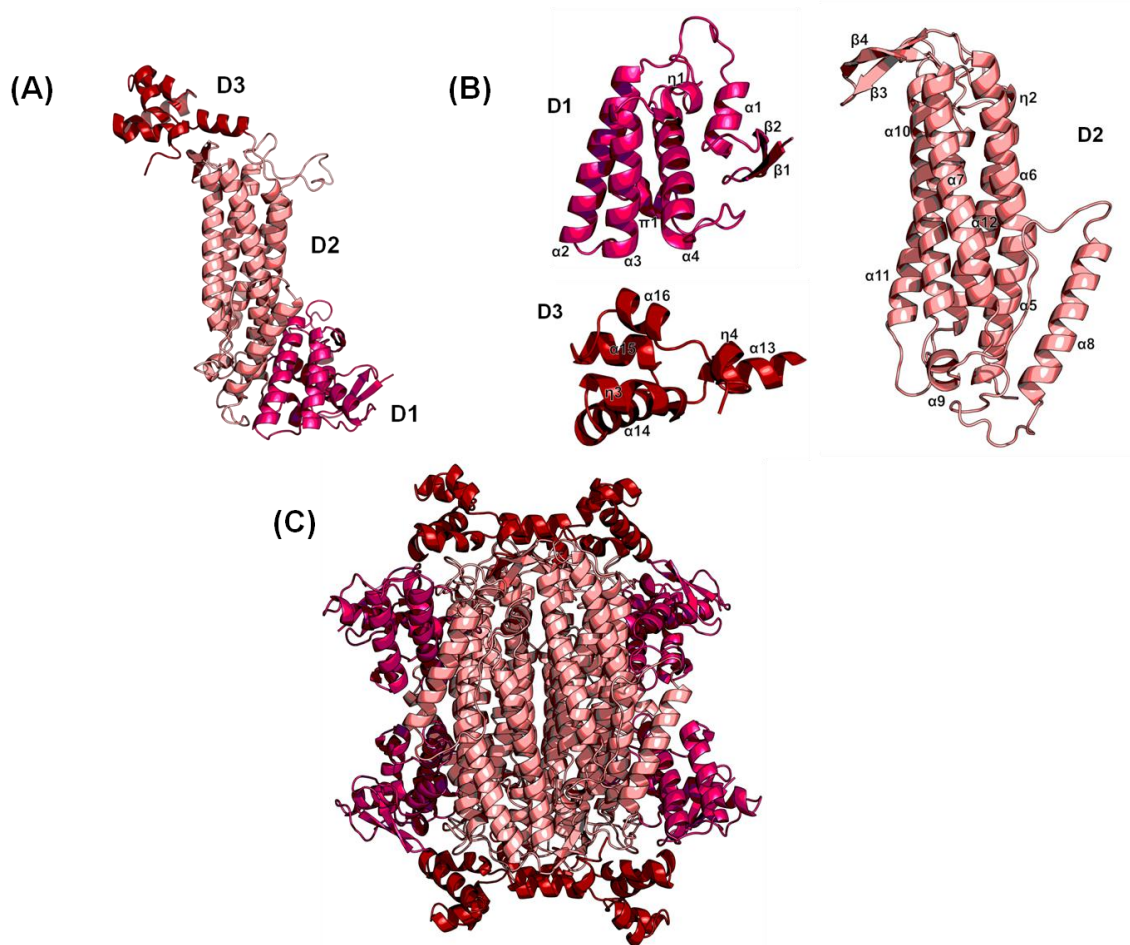


Figure 17. Crystal structure of *SmFHII* solved by molecular replacement (data resolution: 1.85 Å). **(A)** Ribbon diagram of *SmFHII* monomer with D1 colored in pink, D2 colored in salmon, D3 colored in red. **(B)** Ribbon diagram of *SmFHII* domains (D1 - N-terminal domain; D2 - central domain; D3 - C-terminal domain). **(C)** Overall structure of functional tetramer.

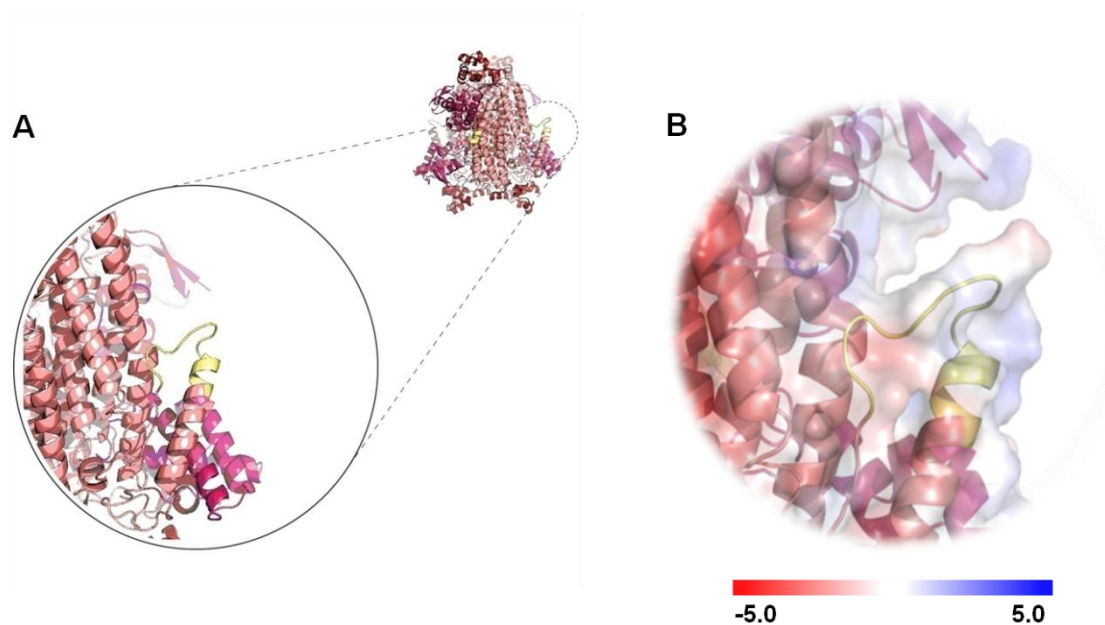


Figure 18. Protuberant additional portion of *SmFHII*. **(A)** Cartoon representation of *SmFHII* structure evidencing the solvent exposed insertion (colored in yellow). **(B)** ± 5 kT/e electrostatic potential surface evidencing the polar residues that compose the protuberant portion (colored in yellow).

The catalytic pocket is composed by two conserved binding sites (A and B). The active site (A site), composed by residues that belong to three of four subunits of tetramer, comprises the catalytic residues His195, Ser340, Lys346, and Glu353. The noncatalytic B site is a shallow region comprising the residues His136 to Asn142. The A and B sites are separated by approximately 12 Å (**Figure 19A**). In our structure, there is one L-malate molecule in each A site, and has closely contact with the residues Ser105, Thr107, Ser146, Ser147, Asn148, His195, Thr194, Ser340, Ser341, Lys346, and Asn348 (**Figure 19B**).

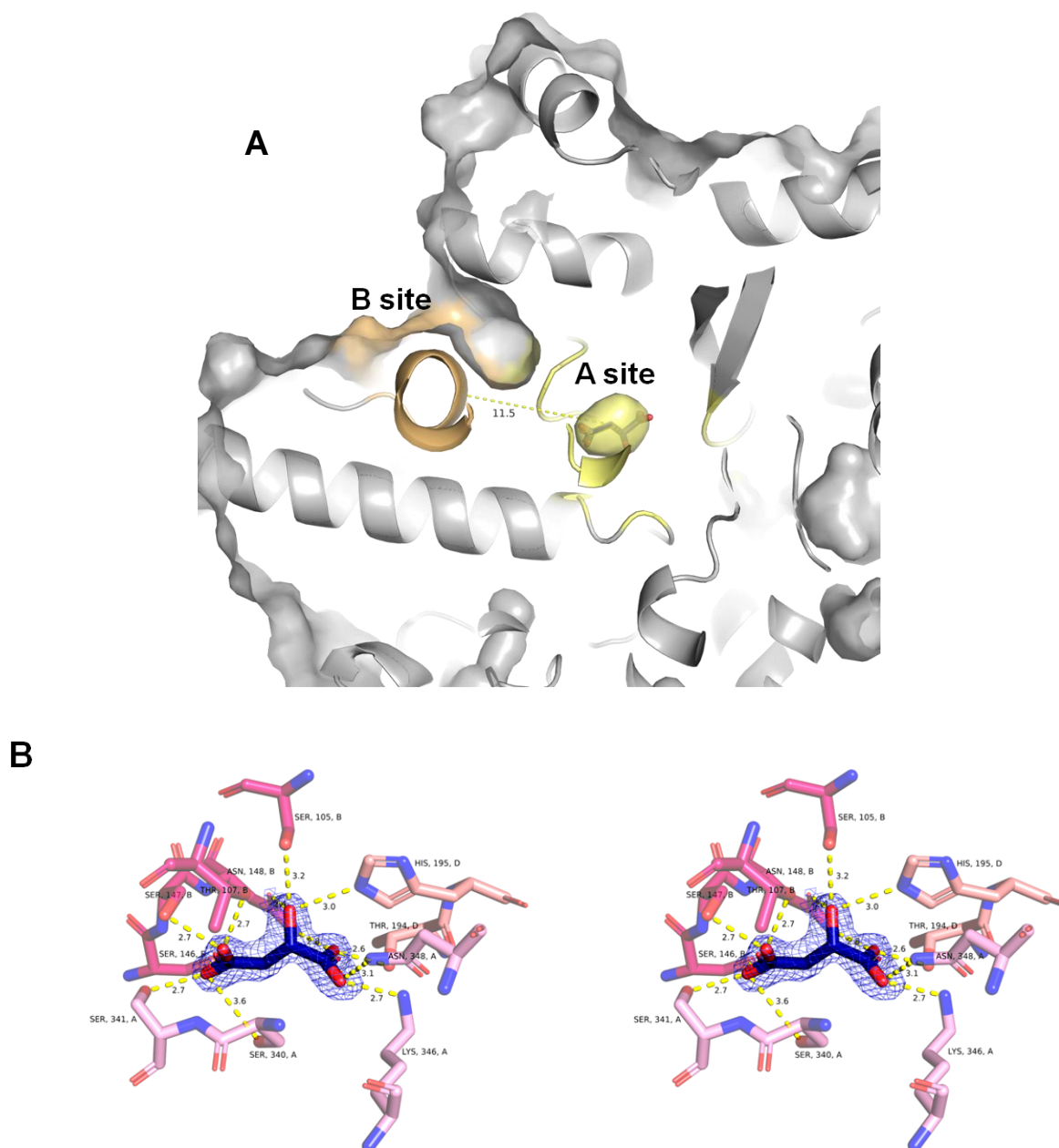


Figure 19. The catalytic pocket. **A** - Distance between the two conserved binding sites: B site (colored in orange) and A site (colored in yellow), estimated by measuring the distance between α -carbon from His140 and C3 from L-malate. **B** - Stereoview of interactions between residues from active site and L-malate molecule. The residues of chains A, B and D are shown in light pink, magenta and salmon, respectively. The substrate L-malate is shown in dark blue, and the interactions between residues and L-malate are shown as yellow dashed lines. Mesh represents the final $2F_o - F_c$ electron density map contoured at 1.2σ level (blue) for L-malate.

The superposition of $C\alpha$ atoms between individually chains of *SmFH_{II}* and *HsFH* allow us to compare the differences in the structure by calculating the root-mean-square deviation (RMSD). As can be visualized (**Figure 20**), the highest RMSD values, and therefore the main structural differences, are in the regions related to the catalytic pocket (B site and

SS-loop). It was not possible to calculate the RMSD between the c-terminal regions due to the differences in conformation that preclude the proper superposition.

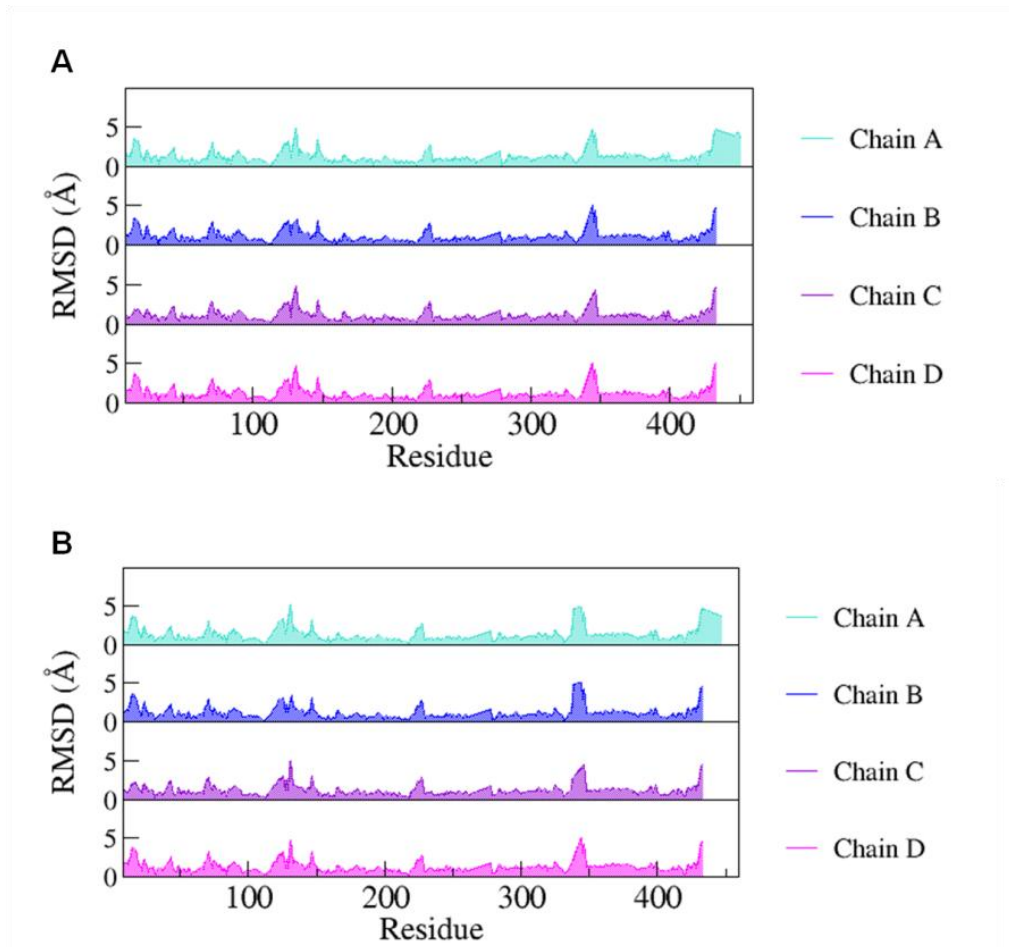


Figure 20. RMSD versus residue. Chains A (cyan), B (blue), C (purple) and D (pink) of SmFHIII against chain A (A) and B (B) from HsFH (5UPP).

5. DISCUSSION

Nowadays, there are 240 million people around the world suffering from schistosomiasis symptoms, which makes extremely necessary the development of a new potent therapy, capable of reducing the parasite infection.

This study comprises the first characterization of the cytosolic class II fumarase from *S. mansoni*, as an important step to exploit its potential as a target for drug discovery efforts against schistosomiasis. This work focused on kinetic and structural studies that contribute to the understanding regarding its mechanism of action as well as provide a pipeline for further drug discovery development.

Schistosoma spp., and also other parasites, resembles tumors tissues due to its intense metabolic activity and high level of cell division for egg production. As a normal cellular process, genome of cell is continuously damaged, and cells with a high metabolism rate can be even more affected⁷¹. Maintaining genome integrity is one of the most important concerns/issues of all living organisms, and failure repairing DNA damage can compromise the whole cell function⁷². For this reason, enzymes involved in DNA repair can be studied as a target to treat schistosomiasis.

The cytosolic fumarase was shown to be a member of DDR. In human cells, to promote DSB repair, fumarase is phosphorylated on Thr236 by the DNA-dependent protein kinase (DNA-PK) complex, inducing the recruitment from the cytosol to the nucleus and local generation of fumarate. Fumarate is responsible for inhibit the lysine demethylase 2B (KDM2B), facilitating the dimethylation of histone H3 on lysine 36 (H3K36me2) by the SET domain and mariner transposase fusion protein (SETMAR). This process leads to the repair of the break by the non-homologous end joining (NHEJ) pathway. In yeast, cytosolic fumarase produces fumarate that regulate the protein level of the resection factor Sae2, that is one of the enzymes involved in DSB resection process in the homologous recombination (HR) repair pathway⁷³.

The inactivity of fumarase impairs DNA repair and can lead to large chromosomal rearrangements, such as deletions, translocations and insertions⁷³. Thus, fumarase has been appointed as a critical element for the DDR to DSBs^{74; 75}.

The absence of fumarase can lead to massive accumulation of fumarate in cells, leading to succination of several proteins and metabolites. Succination is a covalent chemical modification of both cysteine thiol containing metabolites and proteins, which affects their function. It was previously demonstrated that the absence of fumarase in *M. tuberculosis* causes succination of two major antioxidants (catalase and mycothiol), increasing the susceptibility to oxidative stress^{76; 77}. In some cell lines that lacks fumarase activity, the succination of glutathione (GSH), a redox buffer eukaryotic and also many prokaryotic cells, has been observed during fumarate accumulation⁷⁸. GSH is a substrate for glutathione reductase (or thioredoxin glutathione reductase (TGR) in *S. mansoni* and other parasitic flatworms) and its thiol group is able to reduce reactive oxygen species to neutralize them. Studies performed by Zheng et al indicated that succination causes a depletion of GSH, and increase oxidative stress⁷⁹. In fact, TGR from *S. mansoni* have been explored as a drug target, and studies demonstrated that it is essential for parasite survival⁸⁰.

Fumarase is an enzyme extensively interconnected with different metabolic routes, and its inhibition can impact multiple pathways⁷⁷. In this way, *SmFH_{II}* inhibition could impair the DNA repair, causing genomic instability, and also could induce protein and metabolite succination, leading to parasite intoxication and compromising de redox control.

The gene of *SmFH_{II}* is expressed in all life stages of the parasite, being majorly expressed in schistosomules and adult female worms when compared with the other parasitic forms⁸¹.

The search for a selective *SmFH_{II}* inhibitor is a challenging process, since both A and B sites are fully conserved and the search for alternative allosteric regions would be necessary. However, the efforts to find an allosteric selective inhibitor were successfully achieved for *M. tuberculosis* fumarase (*MtFH*)⁵², indicating that exploiting biochemical and structural differences between the pathogen and the human enzyme is achievable in the process of structure-based drug design. Compared with *SmFH_{II}*, this region, found as an allosteric site in *MtFH*, display significant differences. The amino acids residues involved in the interaction with the *MtFH* inhibitor (*N*-(5-(azepan-1-ylsulfonyl)-2-methoxyphenyl)-2-(4-oxo-3,4-dihydrophthalazin-1-yl)acetamide) are not conserved (Lys419, Ser451 and Lys454 in *SmFH_{II}* instead of His397, Leu429 and Arg432 in *MtFH*), precluding the binding of this inhibitor in *SmFH_{II}*. In fact, when *MtFH* inhibitor was tested on *SmFH_{II}*, no inhibition was observed (data not shown). Despite that, this region in *SmFH_{II}* is also a potential cavity that differs from *HsFH*, and remains to be further investigated.

Regarding the DSF assays, fumarase ligands (in both A and B sites), such as citrate, succinate, malate, and malonate, demonstrated significant positive thermal shift. Also, sodium acetate buffer at pH 5.5 and glycerol promotes a thermal stabilization in both *SmFH_{II}* and *SmFH_{II}(Δ 263-277)*. Surprisingly, four acetate molecules were found in the *SmFH_{II}* structure (**Figure 21A**), stabilized by interactions with residues from α -helices of D2 (Ser300, Thr369, Asn390 and Thr394), and four glycerol molecules in two distinct pockets (**Figure 21B**) (two molecules interacting with residues Asn365 and His393 in the side pocket, and other two with L333, Val347 and Pro349 in the top pocket). The results corroborate with the evidence that ligands can be identified with this useful technique. Moreover, since substrate analogues, such as citrate and succinate, can stabilize the protein even at acidic pHs, it is tempting to speculate that loss observed in protein activity at low pHs is not due to the inability of the enzyme in accommodating the substrate, but due to the protonation of a basic group required for the enzymatic reaction⁶⁷.

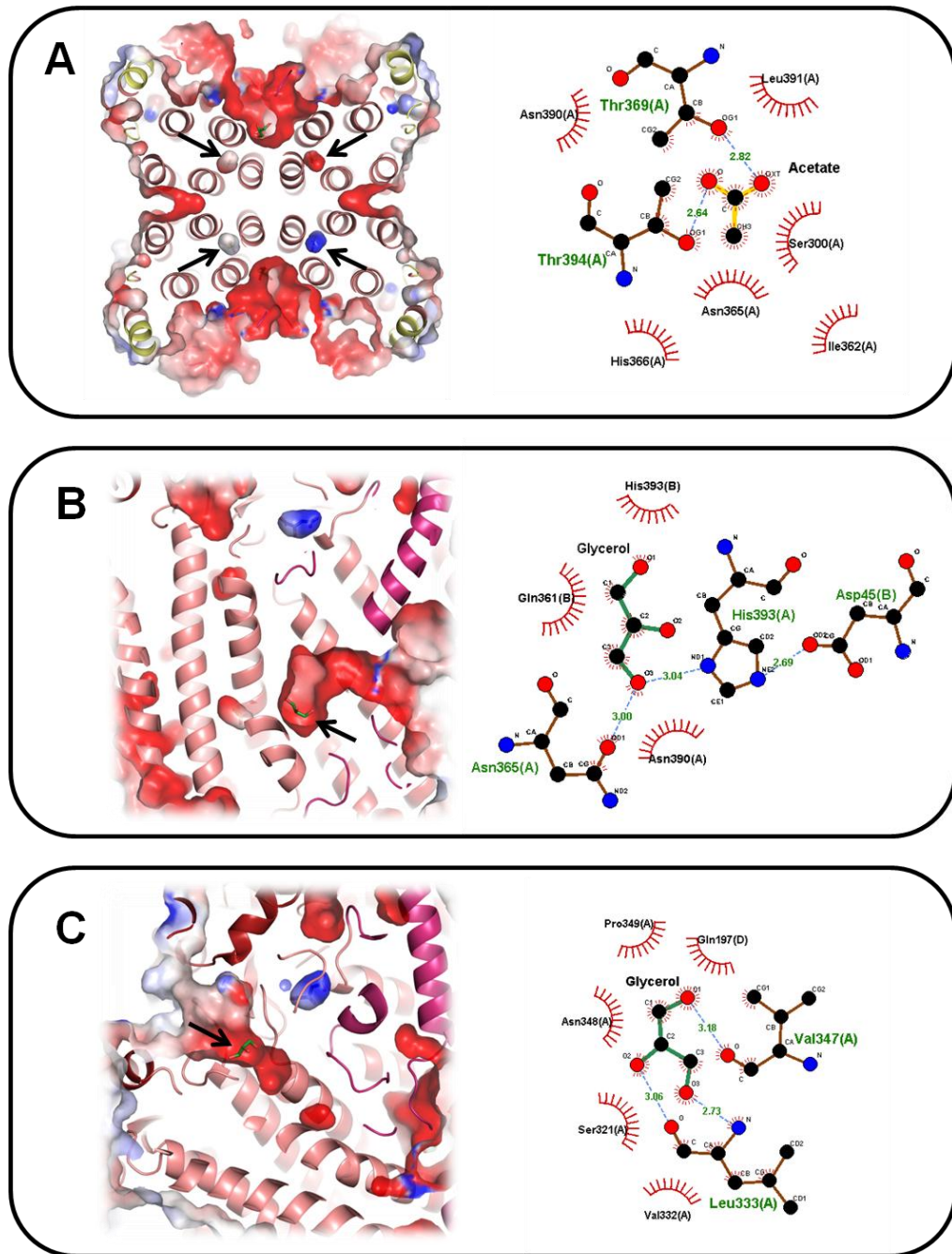


Figure 21. Ligands bound to *SmFH_{II}* structure. (A) Acetates molecules bound in the center of the α -helices (highlighted by black arrows). Interactions between acetate and residues Thr369 and Thr394 are shown in the LigPlot representation. (B) Glycerol molecule bound in a pocket closer to the N-terminal domain (highlighted by black arrow). Interactions between glycerol and residues Asn365 and His393 are shown in the LigPlot representation. (C) Glycerol molecule bound in a pocket near to C-terminal (highlighted by black arrow). Interactions between glycerol and residues Leu333 and Val347 are shown in the LigPlot representation. In all LigPlot representations, the C, N and O atoms are shown in black, blue and red, respectively, and the hydrogen bonds are shown as blue dashed lines.

Although other fumarases have been catalytically characterized, particularities in the experimental set up for each individual enzyme do not allow proper comparison. The steady-state kinetic parameters were estimated taking into account the reversible reaction in the Michaelis–Menten mechanism. K_m values obtained for *SmFH_{II}* are similar to the K_m values observed for the human fumarase under the same conditions, those results are in agreement with the fact that the A site was found fully conserved. However, k_{cat} values are almost 7-10 times lower when compared to *HsFH*. Some studies have demonstrated that amino acids near the SS-loop can determine the maximum rate of reaction of fumarases^{82; 83}. The amino acid substitutions near to the SS-loop can decrease k_{cat} values, with no effect observed for K_m values, probably due the change on electrostatic surface and losses in SS-loop conformational mobility⁸⁴. Based on this, we believe that lower k_{cat} values for *SmFH_{II}* when compared to *HsFH* can be explained by the differences between the amino acids residues found near to the SS-loop.

This work is the first to report the *S. mansoni* class II fumarase structure. Overall, the structure of *SmFH_{II}* is similar to other class II fumarases: a functional tetramer composed mostly by α -helices. Amino acid substitutions between *SmFH_{II}* and *HsFH* are distributed all over the structure, causing subtle changes in protein charge distribution (**Figure 22A**). *SmFH_{II}* has a larger volume than *HsFH* (280527.6 Å³ and 251711.3 Å³, respectively) and is mostly negatively charged at neutral pH. The main differences in the charge distribution can be summarized in three different regions (sites), named S1, S2 and S3 (**Figure 22B**). The S1 involves the α -helices where D2 are connected, and present a pocket formed by different residues from two different chains (residues Pro152-Leu156, Leu228-Ala233, and Glu284-Ala295 from one chain, and Val212-Gln214 from the other chain) and that is not observed in the human fumarase. S2 comprises the meeting point of D3, and forms a cavity where an allosteric inhibitor site was described for *M. tuberculosis* fumarase⁵². The S2 is composed by residues from a C-terminal α -helix (Lys419, Glu422, Tyr423 and Lys426) and a loop (Asn325-Glu330) of two different chains. S3 involves non conservative residues that forms a cavity in the D1 meeting point between two different chains (residues Val40-Asp45, Gln361-Ser370, Ala389-Leu397). S3 contains a deep cavity that has some differences regarding its residues composition when compared to human fumarase. In our structure, a glycerol molecule was found bound in this pocket, and the influence of it in the enzyme activity remains to be investigated.

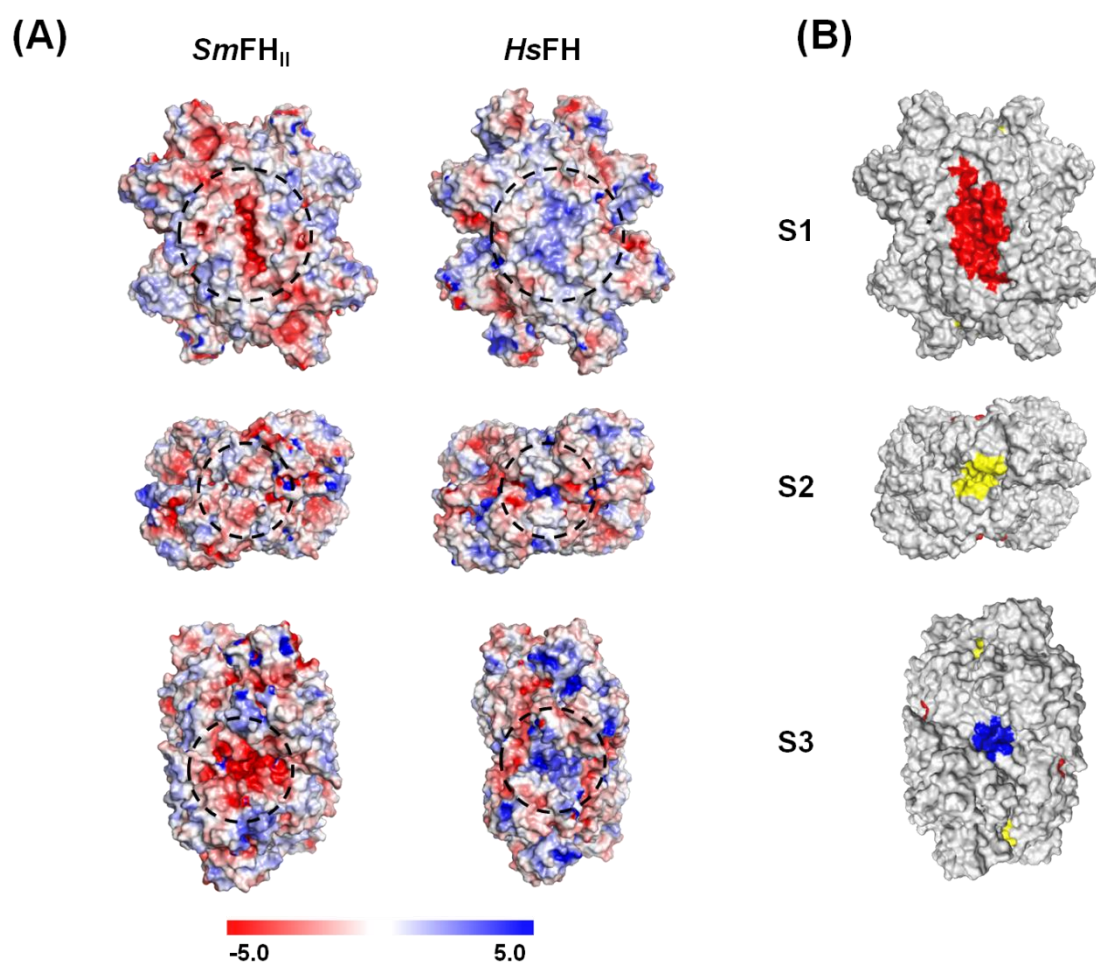


Figure 22. Main differences between *SmFH_{II}* and *HsFH* (5UPP) electrostatic potential surface. (A) - ± 5 kT/e electrostatic potential surface of *SmFH_{II}* and *HsFH* (5UPP), calculated at pH 7.5. (B) - Regions (sites) identified in the charge distribution and topographical analysis. S1 are highlighted in red, S2 in yellow, and S3 in blue.

The presence of L-malate at the active site of *SmFH_{II}* was successfully achieved using cocrystallization method. The experiment was performed at pH 4, in which the enzyme is not able to convert L-malate to fumarate. Thus, the molecule of L-malate remains at the active site, trapped by interactions with the residues of the catalytic pocket. Only two other structures with L-malate in active site are reported (*M. tuberculosis* fumarase - PDB code: 4ADL⁵¹ and *M. abscessus* fumarase - PDB code: 3RRP⁸⁵). All of them have the same close protein-ligand contacts with the equivalent amino acid residues, reinforcing the fact that the substrate conformation is a key part of the catalysis process. In fact, when compared with a structure that possesses fumarate instead of L-malate (*MtFH* S318C mutant, PDB ID: 4APB), we observed the same substrate positioning, indicating that L-malate rearranges to adopt the same conformation of fumarate, in order to establish the same close contacts.

Mechaly et al⁵¹ demonstrated that class II fumarases can adopt two distinct states (open and closed), depending on presence or absence of active site ligands. The open state is a conformation where C-terminal domain adopts an orientation that allows the active site to be accessible to solvent and is observed in the structures described in the apo form. In the closed state, the SS-loop covers the active site, interacting with the bound molecule, and part of the C-terminal domain bends and becomes closer to B-site. In our structure the four subunits of *SmFH_{II}* are all found in the closed state, consistently with the presence of L-malate in the active sites. When compared with the human fumarase structure (5UPP), the difference between open and closed state is even more evident (**Figure 23A**). The open state of 5UPP C-terminal is favored by the presence of a HEPES (4-(2-hydroxyethyl)-1-piperazineethanesulfonic acid) molecule in the interface that connects two adjacent asymmetric units, while the closed state of *SmFH_{II}* C-terminal structure is stabilized by the contacts between Asp139 and NH atoms from Tyr440 and between His136 and Asp441 (**Figure 23B**).

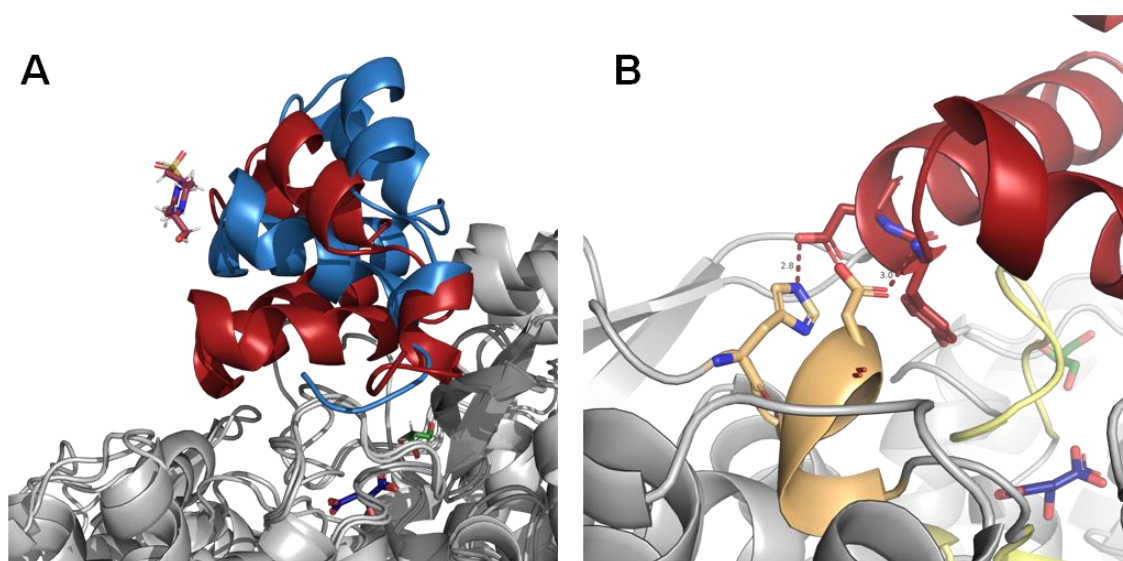


Figure 23. C-terminal closed and open state. **A** - Differences between C-terminal of 6U4O (red) and 5UPP (blue) state. HEPES molecule is shown in pink, L-malate in blue, and glycerol in green. N, O and S atoms are shown in blue, red and yellow, respectively. **B** - *SmFH_{II}* C-terminal structure stabilized by the contacts between Asp139 and Tyr440 and between His136 and Asp441.

In the human fumarase crystal structure (PDB: 5UPP)⁶⁷, His176 side chain (His136 in *SmFH_{II}*) was found pointing towards the entrance of B site, differing from *Escherichia coli* FumC structure in complex with D-malate (PDB: 1FUO)⁴⁹, where a malate molecule was found bound at this site. The D-malate presence at B site induces the reorientation of the histidine side chain (His129 in FumC structure), in order to accommodate the substrate in this

site⁴⁹. In *SmFH_{II}*, the orientation of His136 side chain not only impairs the bound of molecules at the B site, but also contributes to the closed conformation of the C-terminal, as mentioned before (**Figure 23B**).

The additional portion present in the *SmFH_{II}* structure, and also other trematode worms, does not seem to be essential to enzyme activity, since its absence in *SmFH_{II}(Δ 263-277)* construct significantly interfere just in the catalytic constants of L-malate. The protuberant domain is far localized from active site, but apparently has some influence on L-malate binding. Also, the protein stability seems to be compromised by the absence of this portion, since the protein solution presents itself heterogeneous and the thermal stability grossly decreases. The removal of this region causes the break of an α -helix and the loss of interactions between residues, which impairs the protein stability. In fact, all our attempts to crystallize the *SmFH_{II}(Δ 263-277)* were unsuccessful, indicating that the presence of this protuberant portion has relevant influence in protein stability and homogeneity in solution.

Although there is no functional evidence that justify the presence of this prominent domain, we speculate the possibility of this insertion to be related to protein-protein interactions. Protein interactions are fundamental to control the most of cellular processes, including post-translational modifications (phosphorylation, glycosilation, methylation, among others)⁸⁶. In order to investigate the potential of this additional portion as a post-translational modification region, we submitted the *SmFH_{II}* sequence for an in silico analysis. Interestingly, the analysis performed using the NetPhos 3.1 tool⁸⁷ suggests the presence of a phosphorylation site at residue Thr273 (score of 0.979, on a scale of 0 to 1), present in this insert. In humans, fumarase is phosphorylated on Thr236 by the DNA-PK and then is recruited to the nucleus to DSB. *SmFH_{II}* does not possess the equivalent Thr236 at the same position, so we speculated that the Thr273 could be phosphorylated to promote the recruitment of *SmFH_{II}* to the nucleus, in order to act as member of DDR. Although speculative, this result suggests that the additional portion comprising the residues 263 to 277 in *SmFH_{II}* structure could have an important functional role, maybe related to the recruitment of fumarase to the DSB.

6. CONCLUSION

This work presents the first step towards structural and kinetic characterization recombinant cytosolic class II fumarase from *Schistosoma mansoni* (*SmFH_{II}*).

We successfully established a protocol for *SmFH_{II}* expression in *E. coli* BL21(DE3), and we obtained soluble protein with a good yield. The gel filtration chromatography showed that the enzyme is tetrameric, as expected for class II fumarases.

Differential Scanning Fluorometry (DSF) was performed to quantify the change in thermal denaturation temperature under varying pH and salt concentrations, and the results reveal that pH 7.5 and high salt concentration increases the thermal stability of *SmFH_{II}*. Also the DSF has proved to be a useful technique to find new ligands.

We also determined the optimal pH for *SmFH_{II}* activity, and the results indicates that the maximum activity is reached in the range (7 and 7.5) using fumarate as substrate, and pH 8 using L-malate. Enzyme kinetics using both substrates (L-malate and fumarate) were performed, and the results reveal K_m of 0.56 ± 0.08 mM and 0.15 ± 0.02 mM for L-malate and fumarate, respectively. Comparing with the human fumarase, the K_m values were found to be similar, although the k_{cat} values were much higher for *HsFH* than *SmFH_{II}*, probably due the differences between the residues around the catalytic pocket.

The additional portion present in the *SmFH_{II}* structure, and also other trematode worms, is a prolongation of an α -helix and part of a loop that seems not to be essential to enzyme activity, but its absence compromises the protein stability.

SmFH_{II} crystals were obtained using PEG as precipitant agent, and the structure was solved for the first time, by molecular replacement at 1.85 Å, complexed with its substrate L-malate. The final structure was deposited in PDB (accession code 6U4O).

Although class II fumarases share a high level of structural similarity, the main differences between *SmFH_{II}* and *HsFH* structure could be explored to map new allosteric sites and design selective inhibitors.

The results obtained are promising and consisted in the development of a new pipeline to evaluate the potential of *SmFH_{II}* as a drug target against schistosomiasis.

7. REFERENCES

- 1 ORGANIZATION, W. H. Neglected tropical diseases. Disponível em: < https://www.who.int/neglected_diseases/en/ >. Acesso em: Aug 17, 2019.
- 2 BODIMEADE, C.; MARKS, M.; MABEY, D. Neglected tropical diseases: elimination and eradication. **Clinical Medicine**, v. 19, n. 2, p. 157-160, 2019. ISSN 1470-2118.
- 3 Centers for Disease Control and Prevention. Disponível em: < <https://www.cdc.gov/> >. Acesso em: Jun 27, 2019.
- 4 SOUZA, F. et al. Esquistossomose mansônica: aspectos gerais, imunologia, patogênese e história natural. **Rev Bras Clin Med**, v. 9, n. 4, p. 300-7, 2011.
- 5 DEELDER, A. et al. Detection of schistosome antigen in mummies. **Lancet (British edition)**, v. 335, n. 8691, p. 724-725, 1990. ISSN 0140-6736.
- 6 BOUCHET, F. et al. First recovery of *Schistosoma mansoni* eggs from a latrine in Europe (15–16th centuries). **Journal of Parasitology**, v. 88, n. 2, p. 404-406, 2002. ISSN 0022-3395.
- 7 DI BELLA, S. et al. History of schistosomiasis (bilharziasis) in humans: from Egyptian medical papyri to molecular biology on mummies. **Pathogens and global health**, v. 112, n. 5, p. 268-273, 2018. ISSN 2047-7724.
- 8 TAN, S.; AHANA, A. Theodor Bilharz (1825-1862): discoverer of schistosomiasis. **Singapore medical journal**, v. 48, n. 3, p. 184, 2007. ISSN 0037-5675.
- 9 PIRAJÁ DA SILVA, M. Contribuição para o estudo da schistosomiase na Bahia. **Brasil Med**, v. 22, p. 281-283, 1908.
- 10 SAÚDE, M. D. Vigilância da esquistossomose mansoni: diretrizes técnicas. **Biblioteca Virtual em Saúde do Ministério da Saúde**, 2014.
- 11 ORGANIZATION, W. H. Schistosomiasis.
- 12 _____. Schistosomiasis - Fact sheet, 2019.
- 13 HAY, S. I. et al. Global, regional, and national disability-adjusted life-years (DALYs) for 333 diseases and injuries and healthy life expectancy (HALE) for 195 countries and territories, 1990–2016: a systematic analysis for the Global Burden of Disease Study 2016. **The Lancet**, v. 390, n. 10100, p. 1260-1344, 2017. ISSN 0140-6736.

- 14 SAÚDE, M. D. Esquistossomose: causas, sintomas, tratamento, diagnóstico e prevenção. Disponível em: < <http://www.saude.gov.br/saude-de-a-z/esquistossomose> >. Acesso em: Aug 17, 2019.
- 15 NASCIMENTO, G. L. et al. The cost of a disease targeted for elimination in Brazil: the case of schistosomiasis mansoni. **Memórias do Instituto Oswaldo Cruz**, v. 114, 2019. ISSN 0074-0276.
- 16 Esquistossomose. Situação Epidemiológica - Dados. Portal da Saúde 2014.
- 17 WANG, W.; WANG, L.; LIANG, Y.-S. Susceptibility or resistance of praziquantel in human schistosomiasis: a review. **Parasitology research**, v. 111, n. 5, p. 1871-1877, 2012. ISSN 0932-0113.
- 18 WANG, T. et al. Proteomic analysis of the Schistosoma mansoni miracidium. **PLoS one**, v. 11, n. 1, p. e0147247, 2016. ISSN 1932-6203.
- 19 KING, C. H. Toward the elimination of schistosomiasis. **New England Journal of Medicine**, v. 360, n. 2, p. 106-109, 2009. ISSN 0028-4793.
- 20 DOENHOFF, M. J.; CIOLI, D.; UTZINGER, J. Praziquantel: mechanisms of action, resistance and new derivatives for schistosomiasis. **Current opinion in infectious diseases**, v. 21, n. 6, p. 659-667, 2008. ISSN 0951-7375.
- 21 PAX, R.; BENNETT, J.; FETTERER, R. A benzodiazepine derivative and praziquantel: effects on musculature of Schistosoma mansoni and Schistosoma japonicum. **Naunyn-Schmiedeberg's archives of pharmacology**, v. 304, n. 3, p. 309-315, 1978. ISSN 0028-1298.
- 22 KOHN, A. et al. Specific sites in the beta interaction domain of a schistosome Ca²⁺ channel β subunit are key to its role in sensitivity to the anti-schistosomal drug praziquantel. **Parasitology**, v. 127, n. 4, p. 349-356, 2003. ISSN 1469-8161.
- 23 BECKER, B. et al. Light and electron microscopic studies on the effect of praziquantel on Schistosoma mansoni, Dicrocoelium dendriticum, and Fasciola hepatica (Trematoda) in vitro. **Zeitschrift für Parasitenkunde**, v. 63, n. 2, p. 113-128, 1980. ISSN 0044-3255.
- 24 BENIGUEL, L. et al. Differential production in vitro of antigen specific IgG1, IgG3 and IgA: a study in Schistosoma haematobium infected individuals. **Parasite Immunol**, v. 25, n. 1, p. 39-44, Jan 2003. ISSN 0141-9838 (Print) 0141-9838.

- 25 RIVEAU, G. et al. Safety and immunogenicity of rSh28GST antigen in humans: phase 1 randomized clinical study of a vaccine candidate against urinary schistosomiasis. **PLoS Negl Trop Dis**, v. 6, n. 7, p. e1704, 2012. ISSN 1935-2727.
- 26 TRAN, M. H. et al. Tetraspanins on the surface of *Schistosoma mansoni* are protective antigens against schistosomiasis. **Nat Med**, v. 12, n. 7, p. 835-40, Jul 2006. ISSN 1078-8956 (Print) 1078-8956.
- 27 HOTEZ, P. J. et al. Developing vaccines to combat hookworm infection and intestinal schistosomiasis. **Nat Rev Microbiol**, v. 8, n. 11, p. 814-26, Nov 2010. ISSN 1740-1526.
- 28 TENDLER, M. et al. Current status of the Sm14/GLA-SE Schistosomiasis vaccine: overcoming barriers and paradigms towards the first anti-parasitic Human (itarian) vaccine. **Tropical medicine and infectious disease**, v. 3, n. 4, p. 121, 2018.
- 29 FERREIRA, L. G.; OLIVA, G.; ANDRICOPULO, A. D. Target-based molecular modeling strategies for schistosomiasis drug discovery. **Future Med Chem**, v. 7, n. 6, p. 753-64, 2015. ISSN 1756-8919.
- 30 NONATO, M. C. et al. Structural basis for the design of selective inhibitors for *Schistosoma mansoni* dihydroorotate dehydrogenase. **Biochimie**, v. 158, p. 180-190, 2019. ISSN 0300-9084.
- 31 CALIL, F. A. et al. Ligand-based design, synthesis and biochemical evaluation of potent and selective inhibitors of *Schistosoma mansoni* dihydroorotate dehydrogenase. **Eur J Med Chem**, v. 167, p. 357-366, Apr 1 2019. ISSN 0223-5234.
- 32 SERRÃO, V. H. B. et al. Structure and kinetics assays of recombinant *Schistosoma mansoni* dihydrofolate reductase. **Acta tropica**, v. 170, p. 190-196, 2017. ISSN 0001-706X.
- 33 MAREK, M. et al. Structural basis for the inhibition of histone deacetylase 8 (HDAC8), a key epigenetic player in the blood fluke *Schistosoma mansoni*. **PLoS pathogens**, v. 9, n. 9, p. e1003645, 2013. ISSN 1553-7374.
- 34 ABDULLA, M.-H. et al. Schistosomiasis mansoni: novel chemotherapy using a cysteine protease inhibitor. **PLoS medicine**, v. 4, n. 1, p. e14, 2007. ISSN 1549-1676.
- 35 MO, A. X. et al. Schistosomiasis elimination strategies and potential role of a vaccine in achieving global health goals. **The American journal of tropical medicine and hygiene**, v. 90, n. 1, p. 54-60, 2014. ISSN 0002-9637.

- 36 LI, T. et al. High-throughput screening against thioredoxin glutathione reductase identifies novel inhibitors with potential therapeutic value for schistosomiasis. **Infectious diseases of poverty**, v. 4, n. 1, p. 40, 2015. ISSN 2049-9957.
- 37 WOODS, S. A.; SCHWARTZBACH, S. D.; GUEST, J. R. Two biochemically distinct classes of fumarase in *Escherichia coli*. **Biochimica et Biophysica Acta (BBA)-Protein Structure and Molecular Enzymology**, v. 954, p. 14-26, 1988. ISSN 0167-4838.
- 38 GUEST, J. R. et al. The fumarase genes of *Escherichia coli*: location of the *fumB* gene and discovery of a new gene (*fumC*). **Microbiology**, v. 131, n. 11, p. 2971-2984, 1985. ISSN 1465-2080.
- 39 FELICIANO, P. R.; DRENNAN, C. L.; NONATO, M. C. Crystal structure of an Fe-S cluster-containing fumarate hydratase enzyme from *Leishmania major* reveals a unique protein fold. **Proceedings of the National Academy of Sciences**, v. 113, n. 35, p. 9804-9809, 2016. ISSN 0027-8424.
- 40 SUZUKI, T. et al. Rat liver mitochondrial and cytosolic fumarases with identical amino acid sequences are encoded from a single gene. **Journal of Biological Chemistry**, v. 264, n. 5, p. 2581-2586, 1989. ISSN 0021-9258.
- 41 NAST, G.; MULLER-ROBER, B. Molecular characterization of potato fumarate hydratase and functional expression in *Escherichia coli*. **Plant physiology**, v. 112, n. 3, p. 1219-1227, 1996. ISSN 1532-2548.
- 42 YOGEV, O.; NAAMATI, A.; PINES, O. Fumarase: a paradigm of dual targeting and dual localized functions. **Febs Journal**, v. 278, n. 22, p. 4230-4242, 2011. ISSN 1742-4658.
- 43 DIK, E. et al. Human Fumarate Hydratase Is Dual Localized by an Alternative Transcription Initiation Mechanism. **Traffic**, v. 17, n. 7, p. 720-732, 2016. ISSN 1600-0854.
- 44 FELICIANO, P. R. et al. Fumarate hydratase isoforms of *Leishmania major*: subcellular localization, structural and kinetic properties. **International journal of biological macromolecules**, v. 51, n. 1, p. 25-31, 2012. ISSN 0141-8130.
- 45 BESTEIRO, S. et al. Succinate secreted by *Trypanosoma brucei* is produced by a novel and unique glycosomal enzyme, NADH-dependent fumarate reductase. **Journal of Biological Chemistry**, v. 277, n. 41, p. 38001-38012, 2002. ISSN 0021-9258.
- 46 YOGEV, O. et al. Fumarase: a mitochondrial metabolic enzyme and a cytosolic/nuclear component of the DNA damage response. **PLoS Biol**, v. 8, n. 3, p. e1000328, 2010. ISSN 1545-7885.

- 47 RATNER, S. Biosynthesis of urea. VI. Enzymatic cleavage of argininosuccinic acid to arginine and fumaric acid. *PARKER ANSLOW, W.* 204: 115-125 p. 1953.
- 48 GOUET, P. et al. ESPript: analysis of multiple sequence alignments in PostScript. **Bioinformatics (Oxford, England)**, v. 15, n. 4, p. 305-308, 1999. ISSN 1460-2059.
- 49 WEAVER, T.; BANASZAK, L. Crystallographic studies of the catalytic and a second site in fumarase C from *Escherichia coli*. **Biochemistry**, v. 35, n. 44, p. 13955-13965, 1996. ISSN 0006-2960.
- 50 FELICIANO, P. R.; DRENNAN, C. L.; NONATO, M. C. Crystal structures of fumarate hydratases from *Leishmania major* in a complex with inhibitor 2-thiomalate. **ACS chemical biology**, v. 14, n. 2, p. 266-275, 2019. ISSN 1554-8929.
- 51 MECHALY, A. E. et al. Conformational changes upon ligand binding in the essential class II fumarase Rv1098c from *Mycobacterium tuberculosis*. **FEBS letters**, v. 586, n. 11, p. 1606-1611, 2012. ISSN 1873-3468.
- 52 KASBEKAR, M. et al. Selective small molecule inhibitor of the *Mycobacterium tuberculosis* fumarate hydratase reveals an allosteric regulatory site. **Proceedings of the National Academy of Sciences**, v. 113, n. 27, p. 7503-7508, 2016. ISSN 0027-8424.
- 53 DE PÁDUA, R. A. et al. Characterisation of the fumarate hydratase repertoire in *Trypanosoma cruzi*. **International journal of biological macromolecules**, v. 102, p. 42-51, 2017. ISSN 0141-8130.
- 54 JAYARAMAN, V. et al. Biochemical characterization and essentiality of *Plasmodium* fumarate hydratase. **Journal of Biological Chemistry**, v. 293, n. 16, p. 5878-5894, 2018. ISSN 0021-9258.
- 55 YOGEV, O. et al. Fumarase: A Mitochondrial Metabolic Enzyme and a Cytosolic/Nuclear Component of the DNA Damage Response. **Plos Biology**, v. 8, n. 3, Mar 2010. ISSN 1544-9173. Disponível em: < <Go to ISI>://WOS:000278125400008 >.
- 56 NIESEN, F. H.; BERGLUND, H.; VEDADI, M. The use of differential scanning fluorimetry to detect ligand interactions that promote protein stability. **Nature protocols**, v. 2, n. 9, p. 2212, 2007. ISSN 1750-2799.
- 57 PEREIRA DE PADUA, R. A.; NONATO, M. C. Cloning, expression, purification, crystallization and preliminary X-ray diffraction analysis of recombinant human fumarase. **Acta Crystallographica Section F: Structural Biology Communications**, v. 70, n. 1, p. 120-122, 2014. ISSN 2053-230X.

- 58 MCPHERSON, A. **Preparation and analysis of protein crystals.** John Wiley & Sons, 1982. ISBN 0471085243.
- 59 LUFT, J. R.; NEWMAN, J.; SNELL, E. H. Crystallization screening: the influence of history on current practice. **Acta Crystallographica Section F: Structural Biology Communications**, v. 70, n. 7, p. 835-853, 2014. ISSN 2053-230X.
- 60 LUFT, J. R.; DETITTA, G. T. A method to produce microseed stock for use in the crystallization of biological macromolecules. **Acta Crystallographica Section D: Biological Crystallography**, v. 55, n. 5, p. 988-993, 1999. ISSN 0907-4449.
- 61 KABSCH, W. Xds. **Acta Crystallographica Section D: Biological Crystallography**, v. 66, n. 2, p. 125-132, 2010. ISSN 0907-4449.
- 62 VAGIN, A.; TEPLYAKOV, A. MOLREP: an automated program for molecular replacement. **Journal of applied crystallography**, v. 30, n. 6, p. 1022-1025, 1997. ISSN 0021-8898.
- 63 COWTAN, K. The "Buccaneer" protein model building software. **CCP4 Newsletter**, v. 44, 2006.
- 64 MURSHUDOV, G. N.; VAGIN, A. A.; DODSON, E. J. Refinement of macromolecular structures by the maximum-likelihood method. **Acta Crystallographica Section D: Biological Crystallography**, v. 53, n. 3, p. 240-255, 1997. ISSN 0907-4449.
- 65 EMSLEY, P. et al. Features and development of Coot. **Acta Crystallographica Section D: Biological Crystallography**, v. 66, n. 4, p. 486-501, 2010. ISSN 0907-4449.
- 66 GENDA, T.; WATABE, S.; OZAKI, H. Purification and characterization of fumarase from *Corynebacterium glutamicum*. **Bioscience, biotechnology, and biochemistry**, v. 70, n. 5, p. 1102-1109, 2006. ISSN 1347-6947.
- 67 AJALLA ALEIXO, M. A. et al. Structural, biochemical and biophysical characterization of recombinant human fumarate hydratase. **The FEBS journal**, v. 286, n. 10, p. 1925-1940, 2019. ISSN 1742-464X.
- 68 KNIEWALD, J.; MILDNER, P. Thermochemistry of fumarase-inhibitor binding. **FEBS letters**, v. 53, n. 2, p. 225-228, 1975. ISSN 1873-3468.
- 69 MASSEY, V. Studies on fumarase. 4. The effects of inhibitors on fumarase activity. **Biochemical Journal**, v. 55, n. 1, p. 172, 1953.

- 70 WEAVER, T. Structure of free fumarase C from *Escherichia coli*. **Acta Crystallographica Section D: Biological Crystallography**, v. 61, n. 10, p. 1395-1401, 2005. ISSN 0907-4449.
- 71 PEREIRA, A. S. et al. Inhibition of histone methyltransferase EZH2 in *Schistosoma mansoni* in vitro by GSK343 reduces egg laying and decreases the expression of genes implicated in DNA replication and noncoding RNA metabolism. **PLoS neglected tropical diseases**, v. 12, n. 10, p. e0006873, 2018. ISSN 1935-2735.
- 72 TURGEON, M.-O.; PERRY, N. J.; POULOGIANNIS, G. DNA damage, repair, and cancer metabolism. **Frontiers in oncology**, v. 8, p. 15, 2018. ISSN 2234-943X.
- 73 LESHETS, M. et al. Fumarase: From the TCA cycle to DNA damage response and tumor suppression. **Frontiers in molecular biosciences**, v. 5, p. 68, 2018. ISSN 2296-889X.
- 74 JIANG, Y. et al. Local generation of fumarate promotes DNA repair through inhibition of histone H3 demethylation. **Nature cell biology**, v. 17, n. 9, p. 1158, 2015. ISSN 1476-4679.
- 75 LESHETS, M. et al. Fumarase is involved in DNA double-strand break resection through a functional interaction with Sae2. **Current genetics**, v. 64, n. 3, p. 697-712, 2018. ISSN 0172-8083.
- 76 EOH, H.; RHEE, K. Y. Multifunctional essentiality of succinate metabolism in adaptation to hypoxia in *Mycobacterium tuberculosis*. **Proceedings of the National Academy of Sciences**, v. 110, n. 16, p. 6554-6559, 2013. ISSN 0027-8424.
- 77 RUECKER, N. et al. Fumarase deficiency causes protein and metabolite succination and intoxicates *Mycobacterium tuberculosis*. **Cell chemical biology**, v. 24, n. 3, p. 306-315, 2017. ISSN 2451-9456.
- 78 SULLIVAN, L. B. et al. The proto-oncometabolite fumarate binds glutathione to amplify ROS-dependent signaling. **Molecular cell**, v. 51, n. 2, p. 236-248, 2013. ISSN 1097-2765.
- 79 ZHENG, L. et al. Fumarate induces redox-dependent senescence by modifying glutathione metabolism. **Nature communications**, v. 6, p. 6001, 2015. ISSN 2041-1723.
- 80 KUNTZ, A. N. et al. Thioredoxin glutathione reductase from *Schistosoma mansoni*: an essential parasite enzyme and a key drug target. **PLoS Medicine**, v. 4, n. 6, p. e206, 2007. ISSN 1549-1676.

- 81 LU, Z. et al. Schistosome sex matters: a deep view into gonad-specific and pairing-dependent transcriptomes reveals a complex gender interplay. **Scientific reports**, v. 6, p. 31150, 2016. ISSN 2045-2322.
- 82 ESTÉVEZ, M. et al. X-ray crystallographic and kinetic correlation of a clinically observed human fumarase mutation. **Protein science**, v. 11, n. 6, p. 1552-1557, 2002. ISSN 0961-8368.
- 83 KATAYAMA, N.; TAKEYA, M.; OSANAI, T. Biochemical characterisation of fumarase C from a unicellular cyanobacterium demonstrating its substrate affinity, altered by an amino acid substitution. **Scientific reports**, v. 9, n. 1, p. 10629, 2019. ISSN 2045-2322.
- 84 WEAVER, T. et al. Alterations within fumarase C reveal newly observed SS Loop conformations. **The FASEB Journal**, v. 33, n. 1_supplement, p. 468.7-468.7, 2019. ISSN 0892-6638.
- 85 BAUGH, L. et al. Increasing the structural coverage of tuberculosis drug targets. **Tuberculosis**, v. 95, n. 2, p. 142-148, 2015. ISSN 1472-9792.
- 86 PAWSON, T.; NASH, P. Assembly of cell regulatory systems through protein interaction domains. **Science**, v. 300, n. 5618, p. 445-452, 2003. ISSN 0036-8075.
- 87 BLOM, N.; GAMMELTOFT, S.; BRUNAK, S. Sequence and structure-based prediction of eukaryotic protein phosphorylation sites. **Journal of molecular biology**, v. 294, n. 5, p. 1351-1362, 1999. ISSN 0022-2836.

APPENDICES

Table S1. Compounds description of Solubility & Stability Screen from Hampton Research used in the DSF analysis of *SmFH_{II}* with the respective thermal shift values.

Kit ID	Category	Compound description	ΔT_m (°C)
B4	Osmolyte	1250 mM Betaine monohydrate	13.31
G2	Salt	350 mM Sodium phosphate monobasic monohydrate, 650 mM Potassium phosphate dibasic	12.43
F3	Salt	125 mM Gadolinium(III) chloride hexahydrate	11.88
F7	Salt	250 mM DL-Malic acid pH 7.0	11.12
E7	Ionic Liquid	12.5% Cholin acetate	10.79
B1	Peptide	250 mM Gly-gly	10.33
B8	Osmolyte	1000 mM Sucrose	10.28
G5	Salt	500 mM Sodium bromide	10.28
E4	Organic Acid	250 mM Succinic acid pH 7.0	10.27
G6	Polyol and Salt	20% Glycerol, 200mM Lithium chloride	10.14
A5	Amino Acid/Derivative	250 mM Glycine	10.02
D4	Chelator	25 mM Ethylenediaminetetraacetic acid disodium salt dihydrate	9.70
E8	Ionic Liquid	12.5% 1-Ethyl-3-methylimidazolium acetate	9.61
A4	Amino Acid/Derivative	125 mM L-Arginine, 125m M L-Glutamic acid	9.54
G7	Polyol	25% Glycerol	9.49
E3	Organic Acid	250 mM Sodium malonate pH 7.0	9.41
B2	Peptide	100 mM Gly-gly-gly	9.33
B6	Osmolyte	1000 mM Xylitol	9.09
E5	Organic Acid	2.5% Tacsimate pH 7.0	8.97
B7	Osmolyte	1000 mM D-Sorbitol	8.72
E11	Salt	250 mM Ammonium sulfate	8.61
F8	Salt	250 mM Lithium citrate tribasic tetrahydrate	8.36
C6	Linker	250 mM Ethylenediamine dihydrochloride	7.92
F6	Salt	250 mM Lithium nitrate	7.80
A11	Amino Acid/Derivative	250 mM L-Argininamide dihydrochloride	7.65
F12	Salt	500 mM Sodium chloride	7.53
H1	Polyol	25% Polypropylene glycol P 400	7.49
C1	Polyamine	250 mM Spermine tetrahydrochloride	7.43
B5	Osmolyte	375 mM D-(+)-Trehalose dihydrate	7.25
G1	Salt	700 mM Potassium chloride	7.19
A7	Amino Acid/Derivative	60 mM L-Histidine	6.88
E12	Salt	250 mM Ammonium chloride	6.86
G4	Salt	700 mM Lithium chloride	6.63
G9	Polyol	5% Polyethylene glycol 200	6.45
F9	Salt	125 mM Ammonium acetate	6.42
E9	Ionic Liquid	12.5% 1-Butyl-3-methylimidazolium chloride	6.07
B3	Peptide	2.5% Tryptone	6.06

D12	Organic Acid	250 mM Taurine	6.02
H9	Cyclodextrin	5 mM (2-Hydroxypropyl)- β -cyclodextrin	5.73
F1	Salt	250 mM Magnesium sulfate hydrate	5.71
A8	Amino Acid/Derivative	250 mM β -Alanine	5.55
C12	Chaotrope	1.5% Hypotaurine	5.50
D9	Non Detergent	500 mM Non Detergent Sulfobetaine 211 (NDSB-211)	5.33
C9	Chaotrope	250 mM N-Methylurea	5.29
A9	Amino Acid/Derivative	250 mM L-Serine	5.16
D5	Metal	50 mM Magnesium chloride hexahydrate, 50mM Calcium chloride dihydrate	5.15
B10	Osmolyte	1250 mM Trimethylamine N-oxide dihydrate	4.90
B9	Osmolyte	250 mM Hydroxyectoine	4.82
A6	Amino Acid/Derivative	250 mM L-Proline	4.72
A10	Amino Acid/Derivative	250 mM L-Arginine ethyl ester dihydrochloride	4.55
G3	Salt	500 mM Sodium sulfate decahydrate	4.36
C3	Linker	250 mM 5-Aminovaleric acid	4.16
F4	Salt	125 mM Cesium chloride	3.92
B11	Osmolyte	1000 mM Methyl- α -D-glucopyranoside	3.80
H6	Polymer	1.5% Polyethylene glycol 8,000	3.79
F5	Salt	125 mM 4-Aminobutyric acid (GABA)	3.62
D8	Non Detergent	500 mM Non Detergent Sulfobetaine 201 (NDSB-201)	3.47
F2	Salt	250 mM Potassium thiocyanate	3.42
A12	Amino Acid/Derivative	250 mM 6-Aminohexanoic acid	3.31
A3	Amino Acid/Derivative	125 mM L-Arginine	2.95
D3	Inhibitor	2.5 mM Benzamidine hydrochloride	2.94
D7	Non Detergent	500 mM Non Detergent Sulfobetaine 195 (NDSB-195)	2.94
H4	Polymer	1.5% Polyethylene glycol monomethyl ether 1,900	2.90
C7	Chaotrope	250 mM Guanidine hydrochloride	2.82
E1	Organic Acid	250 mM Acetamide	2.63
E10	Ionic Liquid	12.5% Ethylammonium nitrate	2.42
H3	Polyol	5% 1,2-Propanediol	2.33
H7	Polymer	1% Polyvinylpyrrolidone K15	1.64
C8	Chaotrope	250 mM Urea	1.58
E6	Ionic Liquid	12.5% Tetraethylammonium bromide	1.56
G8	Polyol	5% Ethylene glycol	1.44
H5	Polymer	1.5% Polyethylene glycol 3,350	1.25
D10	Non Detergent	500 mM Non Detergent Sulfobetaine 221 (NDSB-221)	1.02
G10	Polyol	2.5% Polyethylene glycol monomethyl ether 550	0.35
REF	Water Control	Reference	0.00
B12	Osmolyte	5 mM Triethylene glycol	-0.33
D11	Non Detergent	400 mM Non Detergent Sulfobetaine 256 (NDSB-256)	-1.07
G11	Polyol	2.5% Polyethylene glycol monomethyl ether 750	-1.50
C10	Chaotrope	100 mM N-Ethylurea	-2.08

F10	Salt	125 mM Sodium benzenesulfonate	-3.16
F11	Salt	125 mM Sodium p-toluenesulfonate	-7.23
C11	Chaotrope	15 mM N-Methylformamide	-8.39
D2	Reducing Agent	10 mM GSH (L-Glutathione reduced), 10mM GSSG (L-Glutathione oxidized)	-10.83
C5	Linker	40 mM Adipic acid	-13.54
A2	Precipitate Control	37.5% Trichloroacetic acid	-
C2	Polyamine	250 mM Spermidine	-
C4	Linker	250 mM Glutaric acid	-
D1	Reducing Agent	75 mM TCEP hydrochloride	-
D6	Metal	50 mM Cadmium chloride hydrate, 50mM Cobalt(II) chloride hexahydrate	-
E2	Organic Acid	250 mM Oxalic acid dihydrate	-
G12	Polyol	25% Formamide	-
H10	Cyclodextrin	40 mM α -Cyclodextrin	-
H11	Cyclodextrin	5 mM β -Cyclodextrin	-
H12	Cyclodextrin	25 mM Methyl- β -cyclodextrin	-
H2	Polyol	12.5% Pentaerythritol ethoxylate (15/4 EO/OH)	-
H8	Polymer	50 mM 6-O- α -D-Maltosyl- β -cyclodextrin	-

Table S2. Compounds description of Solubility & Stability Screen from Hampton Research used in the DSF analysis of *SmFH_{II}*(Δ 263-277) with the respective thermal shift values.

Kit ID	Category	Compound description	ΔT_m (°C)
G2	Salt	350mM Sodium phosphate monobasic monohydrate, 650mM Potassium phosphate dibasic	19.65
F1	Salt	250mM Magnesium sulfate hydrate	19.29
F7	Salt	250mM DL-Malic acid pH 7.0	16.74
E11	Salt	250mM Ammonium sulfate	15.27
B8	Osmolyte	1000mM Sucrose	14.35
H6	Polymer	1.5% Polyethylene glycol 8,000	14.24
G6	Polyol and Salt	20% Glycerol, 200mM Lithium chloride	13.27
G3	Salt	500mM Sodium sulfate decahydrate	12.99
E8	Ionic Liquid	12.5% 1-Ethyl-3-methylimidazolium acetate	12.58
G7	Polyol	25% Glycerol	12.45
E7	Ionic Liquid	12.5% Cholin acetate	12.18
G4	Salt	700mM Lithium chloride	12.17
E4	Organic Acid	250mM Succinic acid pH 7.0	11.84
B7	Osmolyte	1000mM D-Sorbitol	11.49
B4	Osmolyte	1250mM Betaine monohydrate	11.25
A4	Amino Acid/Derivative	125mM L-Arginine, 125mM L-Glutamic acid	10.34
D4	Chelator	25mM Ethylenediaminetetraacetic acid disodium salt dihydrate	10.32
B6	Osmolyte	1000mM Xylitol	10.28
D7	Non Detergent Amino	500mM Non Detergent Sulfobetaine 195 (NDSB-195)	10.12
A5	Amino Acid/Derivative	250mM Glycine	9.74
D10	Non Detergent	500mM Non Detergent Sulfobetaine 221 (NDSB-221)	9.68

E12	Salt	250mM Ammonium chloride	9.67
C6	Linker	250mM Ethylenediamine dihydrochloride	9.63
E5	Organic Acid	2.5% Tacsimate pH 7.0	9.59
C1	Polyamine	250mM Spermine tetrahydrochloride	9.24
D8	Non Detergent	500mM Non Detergent Sulfobetaine 201 (NDSB-201)	9.12
B1	Peptide	250mM Gly-gly	8.88
D12	Organic Acid Amino	250mM Taurine	8.76
A9	Acid/Derivative	250mM L-Serine	8.75
B2	Peptide	100mM Gly-gly-gly	8.75
G1	Salt	700mM Potassium chloride	8.67
F9	Salt Amino	125mM Ammonium acetate	8.64
A8	Acid/Derivative	250mM β -Alanine	8.61
G5	Salt	500mM Sodium bromide	8.37
B5	Osmolyte	375mM D-(+)-Trehalose dihydrate	8.34
B10	Osmolyte	1250mM Trimethylamine N-oxide dihydrate	8.1
C12	Chaotrope Amino	1.5 Hypotaurine	7.7
A11	Acid/Derivative	250mM L-Argininamide dihydrochloride	7.52
F12	Salt	500mM Sodium chloride	7.24
F6	Salt	250mM Lithium nitrate	7.07
F11	Salt	125mM Sodium p-toluenesulfonate	6.99
D9	Non Detergent	500mM Non Detergent Sulfobetaine 211 (NDSB-211)	6.31
F8	Salt	250mM Lithium citrate tribasic tetrahydrate	5.46
H7	Polymer	1% Polyvinylpyrrolidone K15	5.31
E3	Organic Acid	250mM Sodium malonate pH 7.0	5.3
E6	Ionic Liquid	12.5% Tetraethylammonium bromide	5.2
G11	Polyol	2.5% Polyethylene glycol monomethyl ether 750	4.97
B9	Osmolyte Amino	250mM Hydroxyectoine	4.41
A12	Acid/Derivative	250mM 6-Aminohexanoic acid	4.22
B12	Osmolyte Amino	5mM Triethylene glycol	4.07
A6	Acid/Derivative	250mM L-Proline	3.64
G9	Polyol Amino	5% Polyethylene glycol 200	3.62
A7	Acid/Derivative	60mM L-Histidine	3.51
G8	Polyol Amino	5% Ethylene glycol	2.62
A10	Acid/Derivative	250mM L-Arginine ethyl ester dihydrochloride	2.56
F5	Salt	125mM 4-Aminobutyric acid (GABA)	2.35
D3	Inhibitor	2.5mM Benzamidine hydrochloride	2.01
D11	Non Detergent	400mM Non Detergent Sulfobetaine 256 (NDSB-256)	2
G10	Polyol	2.5% Polyethylene glycol monomethyl ether 550	1.78
H3	Polyol	5% 1,2-Propanediol	1.55
H5	Polymer	1.5% Polyethylene glycol 3,350	1.48
F4	Salt	125mM Cesium chloride	1.13
H4	Polymer	1.5% Polyethylene glycol monomethyl ether 1,900	0.32

REF	Water		0.02
C10	Chaotrope	100mM N-Ethylurea	-0.9
C9	Chaotrope	250mM N-Methylurea	-1.61
C8	Chaotrope	250mM Urea	-1.63
F10	Salt	125mM Sodium benzenesulfonate	-2.59
E10	Ionic Liquid	12.5% Ethylammonium nitrate	-3.04
C3	Linker	250mM 5-Aminovaleric acid	-3.18
E9	Ionic Liquid	12.5% 1-Butyl-3-methylimidazolium chloride	-3.34
B3	Peptide	2.5% Tryptone	-5.66
A2	Precipitate Control	37.5% Trichloroacetic acid	-
A3	Amino Acid/Derivative	125mM L-Arginine	-
B11	Osmolyte	1000mM Methyl- α -D-glucopyranoside	-
C11	Chaotrope	15mM N-Methylformamide	-
C2	Polyamine	250mM Spermidine	-
C4	Linker	250mM Glutaric acid	-
C5	Linker	40mM Adipic acid	-
C7	Chaotrope	250mM Guanidine hydrochloride	-
D1	Reducing Agent	75mM TCEP hydrochloride	-
D2	Reducing Agent	10mM GSH (L-Glutathione reduced), 10mM GSSG (L-Glutathione oxidized)	-
D5	Metal	50mM Magnesium chloride hexahydrate, 50mM Calcium chloride dihydrate	-
D6	Metal	50mM Cadmium chloride hydrate, 50mM Cobalt(II) chloride hexahydrate	-
E1	Organic Acid	250mM Acetamide	-
E2	Organic Acid	250mM Oxalic acid dihydrate	-
F2	Salt	250mM Potassium thiocyanate	-
F3	Salt	125mM Gadolinium(III) chloride hexahydrate	-
G12	Polyol	25% Formamide	-
H1	Polyol	25% Polypropylene glycol P 400	-
H10	Cyclodextrin	40mM α -Cyclodextrin	-
H11	Cyclodextrin	5mM β -Cyclodextrin	-
H12	Cyclodextrin	25mM Methyl- β -cyclodextrin	-
H2	Polyol	12.5% Pentaerythritol ethoxylate (15/4 EO/OH)	-
H8	Polymer	50mM 6-O- α -D-Maltosyl- β -cyclodextrin	-
H9	Cyclodextrin	5mM (2-Hydroxypropyl)- β -cyclodextrin	-